











Microborings reveal alternating agitation, resting and sleeping stages of modern marine ooids

PHYLLIS MONO*†‡ , RENÉ HOFFMANN† , MAX WISSHAK‡ ,
STEPHEN W. LOKIER§ , CHELSEA L. PEDERSON¶ ,
DOMINIK HENNHOFER** , MARA R. DIAZ†† , PETER K. SWART†† ,
GERNOT NEHRKE‡‡  and ADRIAN IMMENHAUSER†'§§ 

*Institute for Earth System Science and Remote Sensing, University of Leipzig, Talstr. 35, Leipzig 04103, Germany (E-mail: phyllis.mono@uni-leipzig.de)

†Institute of Geology, Mineralogy, and Geophysics, Ruhr-Universität Bochum, Universitätsstrasse 150, Bochum 44801, Germany

‡Marine Research Department, Senckenberg am Meer, Wilhelmshaven 26382, Germany

§School of Built and Natural Environment, University of Derby, Kedleston Road, Derby DE22 1GB, UK

¶School of Ocean Science and Engineering, University of Southern Mississippi, Stennis Space Center, 1020 Balch Boulevard, Kiln, MS 39556, USA

**Hessisches Landesmuseum Darmstadt, Friedensplatz 1, Darmstadt 64283, Germany

††Department of Marine Geosciences, Rosenstiel School of Marine, Atmospheric, and Earth Science, University of Miami, 4600 Rickenbacker Causeway, Miami, Florida 33149, USA

‡‡Alfred-Wegener-Institut Helmholtz-Zentrum für Polar- und Meeresforschung, Bremerhaven 27570, Germany

§§Fraunhofer Research Institution for Energy Infrastructures and Geothermal Systems, Am Hochschulcampus 1, Bochum 44801, Germany

Associate Editor – Jody Webster

ABSTRACT

Ooids are abundant carbonate grains throughout much of Earth's history, but their formation is not well understood. Here, an in-depth study of microbial bioerosion features of Holocene ooids from the Schooner Cays ooid shoals (Great Bahama Bank, Eleuthera, Bahamas) and the Shalil al Ud ooid shoals in the Arabian/Persian Gulf (Abu Dhabi, United Arab Emirates) is presented. No obvious differences were found in ooid size distribution, cortex layer thickness, the composition of nuclei or euendolithic community when comparing ooids from both locations. Microendolithic borings are present in most studied ooid surfaces, but the intensity of (micro-)bioerosion varies significantly. Applying an epoxy vacuum cast-embedding technique allowed the identification of ichnotaxa and their inferred producers (various genera of diatoms, cyanobacteria, coccolithophores and unspecified bacteria). Euen-dolithic taxa have specific low-light tolerances and light optima. This implies that information about the relative bathymetry (seafloor versus burial within an ooid shoal) and ecology for ooid cortex formation can be obtained via the presence or absence of their respective ichnotaxa. The history of a statistically significant number of ooid cortices can be translated into dune dynamics and the temporal variations thereof by allocating the inferred index producer to a defined burial or light penetration zone. In this context, ooid formation can be divided into four stages: (i) an agitation stage in the water column, characterized by the colonization of grains by photoautotrophs; (ii) a resting stage, characterized by temporary burial of the ooid, leading to immobilization and a shift towards heterotrophs; (iii) a sleeping stage, characterized by prolonged burial and colonization by organotrophs;

and (iv) a reactivation stage, characterized by a resurfacing of the ooid and a subsequent shift towards photoautotrophs. The sleeping stage is presumably a stage of ooid degradation where bioerosion, mainly by heterotrophic fungi and bacteria is particularly active.

Keywords Bioerosion, carbonate fabrics, Holocene, ichnotaxa, light penetration, ooids.

INTRODUCTION

Ooids (Sorby, 1879; Kalkowsky, 1908), and their many subtypes, are spherical or ovoidal carbonate grains with concentric laminae coating a carbonate or non-carbonate nucleus (see Diaz & Eberli, 2019). The one to several-micron-thick laminae of calcareous ooids consist of nanometre-sized aragonitic or calcitic batten-like crystals (needles and rods; Richter, 1983; Richter & Neuser, 1998; Scholle & Ulmer-Scholle, 2003; Flügel & Munnecke, 2010; Harris *et al.*, 2019). Ooids have formed abundantly in shallow warm (sub-tropical) marine or lacustrine environments throughout much of Earth's history (Simone, 1980; Rankey & Reeder, 2012; Diaz *et al.*, 2014, 2015, 2017; Diaz & Eberli, 2019). Ooid formation has been particularly abundant when high eustatic sea level flooded continental interiors, forming shallow warm epeiric seas with significant potential for high carbonate saturation (Opdyke & Wilkinson, 1990). While aragonitic rods commonly form tangentially around the nucleus and occur in high-energy settings, calcitic rods form radially and are typically indicative of quiescent water conditions (Davies *et al.*, 1978; Flügel & Munnecke, 2010; Diaz & Eberli, 2019). Previous studies have linked ooid mineralogy to environmental factors, including fluctuations in the Mg/Ca ratio (Sandberg, 1975, 1983; Popp & Wilkinson, 1983; Li *et al.*, 2015). Recent marine ooids have predominantly aragonitic or high-Mg calcite mineralogy, typically reach <2 mm in diameter and are characterized by dull polished surfaces. Modern settings of ooid formation include the Great Bahama Bank, the Yucatan Shelf, the Arabian/Persian Gulf (hereafter referred to as 'the Gulf'), the Gulf of Mexico, and areas of the Red Sea and Shark Bay in Australia. Among these, ooids from the Bahamas are the most iconic and best-studied (e.g. Harris, 1983, 2010; Budd & Land, 1990; Rankey *et al.*, 2006; Reeder & Rankey, 2008; Bergman *et al.*, 2010; Rankey & Reeder, 2011; Diaz *et al.*, 2013a, 2013b, 2014, 2015; Mariotti *et al.*, 2018; Harris *et al.*, 2019).

Despite more than a century of research, ooid formation and alteration in marine settings

remains insufficiently understood. The influence of abiotic factors, including hydrodynamic level, pH, temperature and salinity, and of biotic factors, including geomicrobiological/organomineral processes, is complex (see reviews in Simone, 1980; Diaz & Eberli, 2019; Harris *et al.*, 2019). Suarez-Gonzalez & Reitner (2021) even observed the static formation of aragonitic ooids in microbial mats and attributed their formation to both biological [extracellular polymeric substance (EPS) degradation] and environmental factors (variations in supersaturation in the biomat). In addition, Diaz *et al.* (2014) presented compelling arguments for biologically influenced CaCO₃ precipitation in modern marine ooids, fostered by the synergistic effect of microbes with the potential to dissolve and/or induce micritization on carbonate substrates.

Microbial bioerosion described from ooid surfaces and within cortices includes shallow or deeply penetrating borings and superficial grazing traces (<100 µm tunnel diameter; Glaub *et al.*, 2007; but see Wisshak, 2012). These features have been attributed to euendolithic microorganisms (Vogel *et al.*, 2000; Tapanila, 2008; Radtke & Golubic, 2011). Euendolithic microorganisms are subdivided into those with a phototrophic (for example, cyanobacteria, chlorophytes, rhodophytes and foraminifera) and organotrophic (for example, bacteria and fungi) lifestyle (Glaub *et al.*, 2007). In warm-temperate to tropical settings, microbial bioeroders rapidly colonize the substrate surfaces of biogenic and abiogenic carbonates (Vogel *et al.*, 2000; Gektidis *et al.*, 2007; Tapanila, 2008; Wisshak *et al.*, 2011). Erosion by microborers is assumed to be primarily (bio-)chemical, although the exact mechanisms are still poorly understood (Golubic *et al.*, 1981; Vogel *et al.*, 2000; Gektidis *et al.*, 2007; Tapanila, 2008; Wisshak, 2012). In the trace fossil record, recurrent morphologies of microbioerosion traces (ichnotaxa) and trace communities (ichnocoenoses) can be correlated back to their respective producer by their distinctive shape and size (Vogel *et al.*, 1995, 2000; Glaub, 2004; Gektidis *et al.*, 2007; Glaub *et al.*, 2007; Radtke & Golubic, 2011; Wisshak, 2012). For a

comprehensive overview of all bioerosion ichnotaxa, see Wisshak *et al.* (2019). The typical boring pattern of particular euendolithic organisms provides biological and ecological information about the respective group of trace fossils (Glaub *et al.*, 2007; Tapanila, 2008).

Ooids are often colonized by coccoid euendolithic cyanobacteria, with the most commonly occurring trace originating from the *Hyella* and the *Solentia* genera (Al-Thukair & Golubic, 1991; Al-Thukair *et al.*, 1994; Gektidis, 1997; Glaub *et al.*, 2001; Radtke & Golubic, 2011; Amao & Al-Ramadan, 2018). Previous studies examined the taxonomy of microendolithic assemblages on ooid surfaces from the Bahamas and the Gulf (Harris *et al.*, 1979; Al-Thukair & Golubic, 1991; Al-Thukair *et al.*, 1994; Radtke & Golubic, 2011), the formation of micritic envelopes due to bioerosion by boring microorganisms (e.g. Bathurst, 1966; Margolis & Rex, 1971; Friedman *et al.*, 1971; Golubic *et al.*, 1975; Gaffey, 1983; Glaub *et al.*, 2001; Amao & Al-Ramadan, 2018; Ge *et al.*, 2020a, 2020b) and the significance of ichnospecies as palaeoecological (including water and burial depth) proxies (Golubic *et al.*, 1984, 2016; Vogel *et al.*, 1987, 1995, 1996, 2000; Glaub, 1994; Gektidis, 1997; Glaub & Bundschuh, 1997). Furthermore, the analysis of microborings is a key tool in deciphering the microbiome of biogenic carbonates, such as fossil corals or mollusc shells (e.g. Salamon *et al.*, 2019; Schätzle *et al.*, 2021; Salamon & Kołodziej, 2022).

This paper investigates microendolithic borings on the surface and within the cortex of modern marine ooids from the Schooner Cays shoals (Great Bahama Bank) and the outer lagoon (Shalil al Ud) north-east of Abu-Dhabi (the Gulf). The aims of this paper are: (i) to provide detailed documentation of microendolithic borings in ooid cortices; (ii) to propose an ichnotaxonomic identification of the microendolithic traces and their inferred producers; (iii) to assess the burial depth distribution and cross-cutting relationship of microendoliths within the cortex; and (iv) to reconstruct the chronology of ooid cortex layer formation and bioerosion events in the context of geomicrobial activity and previous ooid formation hypotheses. This work has wide implications, because elucidating the stratigraphy of microendolithic boring intervals within ooid cortices offers the potential to more quantitatively assess ooid growth, resting and sleeping stages in modern carbonate environments. Moreover, data shown here also have a bearing on

understanding ooid shoal dynamics, including the short-term migration of sand waves at the top of the shoal and the resulting long-term effects.

STUDY AREAS AND CASE SETTINGS

Schooner Cays ooid shoals

The Schooner Cays tidal-bar belt (Fig. 1A and C) is located north of Exuma Sound on the Great Bahama Bank, east of the Eleuthera Islands. It extends over 20 × 56 km and is formed by Holocene ooid sands. Various authors (e.g. Ball, 1967; Dravis, 1979; Harris *et al.*, 2011, 2014; Purkis & Harris, 2017; Rush & Rankey, 2017; Purkis *et al.*, 2019) provided detailed descriptions of the physiography, sedimentology, size and evolution of the tidal bar belt, with implications for physical and hydrodynamic controls on deposition as well as stratigraphic and morphometric correlations to other sand bodies. Individual tidal bars consist of up to 1 km wide shoals of ooid sands. The crests of the shoals are partially exposed during low tide for several hours and submerged during high tide. The average water depth atop the shoals during mid-tidal levels is less than 1 m. Salinity at the Great Bahama Bank is 38 to 42‰ and therefore slightly elevated compared to open marine settings (Whitaker & Smart, 1990). The Schooner Cays proper represent stabilized carbonate islands atop several ooid-sand shoals. The Schooner Cays ooid sands (Fig. 2A to E) consist of whitish ooid grains with average diameters between 0.18 mm and 1.0 mm (Fig. 2A). Radiocarbon dating suggests that the ooid formation started approximately 100 to 2800 years BP (Duguid *et al.*, 2010). These large deviations can be explained by the fact that tidal currents still actively formed and transported these ooids.

The Gulf (Shalil al Ud ooid shoals)

The shallow (average depth = 36 m) south-western Gulf (Fig. 1B and D) overlies a low-gradient continental basement and represents a modern subtropical epeiric sea with active carbonate sedimentation (Edinger *et al.*, 2002; Lokier & Fiorini, 2016; Pederson *et al.*, 2021). As part of the south-western Gulf, the Abu Dhabi coastal area comprises a mosaic of shallow lagoons (0 to 10 m deep) and small barrier islands. The complex geography is inherited

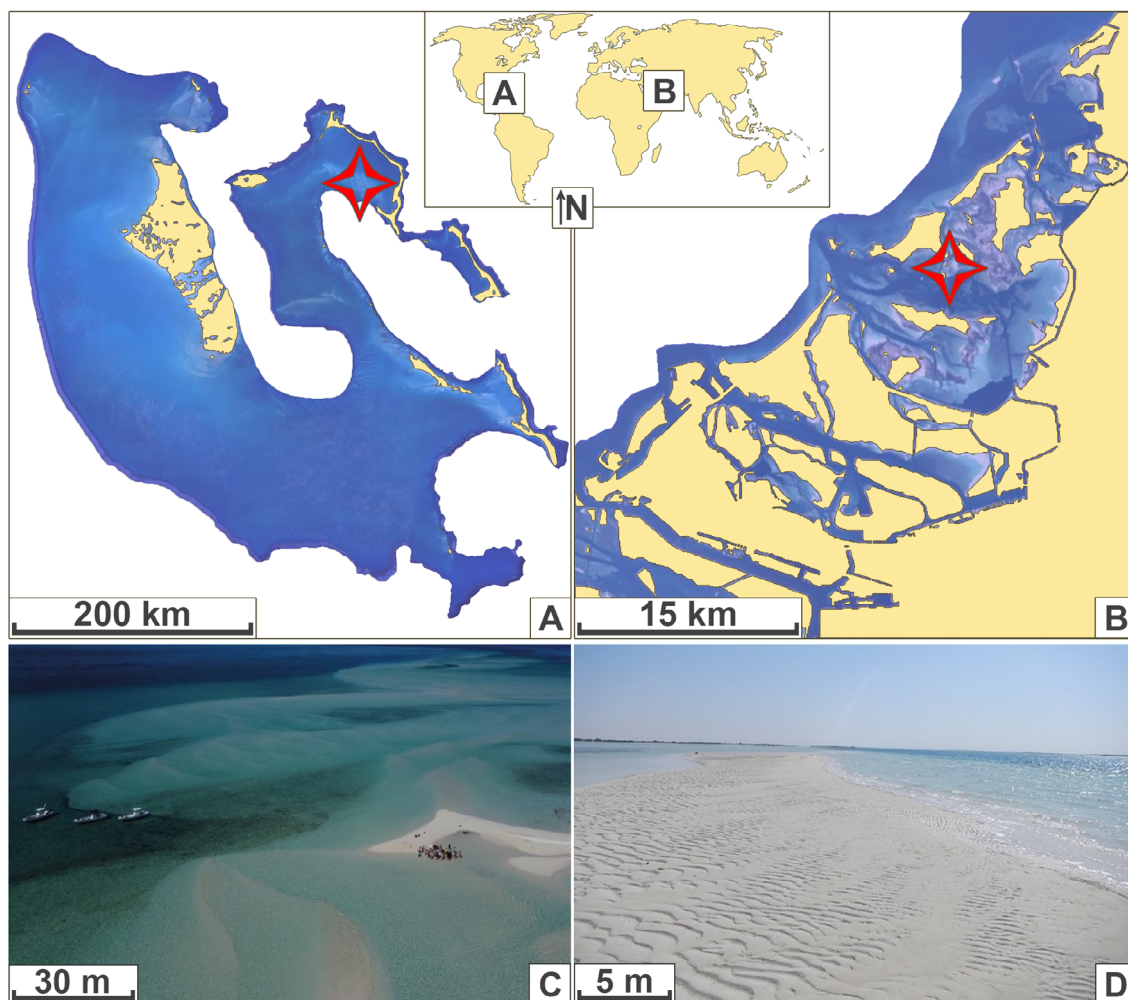


Fig. 1. Location of sampling sites indicated by red stars. (A) Map of the Great Bahama Bank with sampling sites on Schooner Cays ooid shoals, located north of Exuma Sound and east of the Eleuthera Islands. (B) Eastern Gulf, with indication of outer lagoon of Abu-Dhabi (Shalil al Ud, *ca* 20 km north-east of Abu Dhabi city). Small inset on top locates the sampling sites on the world map. (C) Drone images of the Schooner Cays ooid shoals, Bahamas (image courtesy of Drew Dalton). (D) Field image of the Abu-Dhabi outer lagoon shoals (Shalil al Ud), Eastern Gulf.

from eustatic fluctuations during Quaternary glaciation events (Evans *et al.*, 1969; Stevens *et al.*, 2014). The climate in Abu Dhabi is hot and arid, with summer temperatures reaching over 50°C and littoral humidity reaching 100% (Kinsman, 1964; Lokier & Fiorini, 2016). The average rainfall is 72 mm/year, but the average evaporation is 2.75 m/year (Lokier & Fiorini, 2016). The coastal tidal range is small (1 to 2 m), but storm surges often occur due to strong seasonal north–north-westerly winds (Shamals). Seawater salinity in the Gulf is about 40 to 45‰ (Ge *et al.*, 2020a). There has been no riverine influx along the Southern coast of the Gulf since the Early Pleistocene (Arboit *et al.*, 2022).

Ooidal shoals and ooid deltas in the outer lagoon (Shalil al Ud) extend to an area of more than 83 km², forming in a high-energy setting influenced by strong tidal activity. At low tide, the crests of shoals are subaerially exposed for several hours, while at high tide, the shoals are submerged and influenced by tidal currents and wind-generated waves. At these times, ooids are actively formed and transported. The intershoal seafloor is covered by seagrass, which provides a stabilizing effect. The seafloor sediment consists of ooids (60 to 90 vol.%), gastropods, calcareous algae, echinoderms and foraminifera (Ge *et al.*, 2020a, 2020b). The Shalil al Ud ooid sands (Fig. 2F to J) consist of white-tan

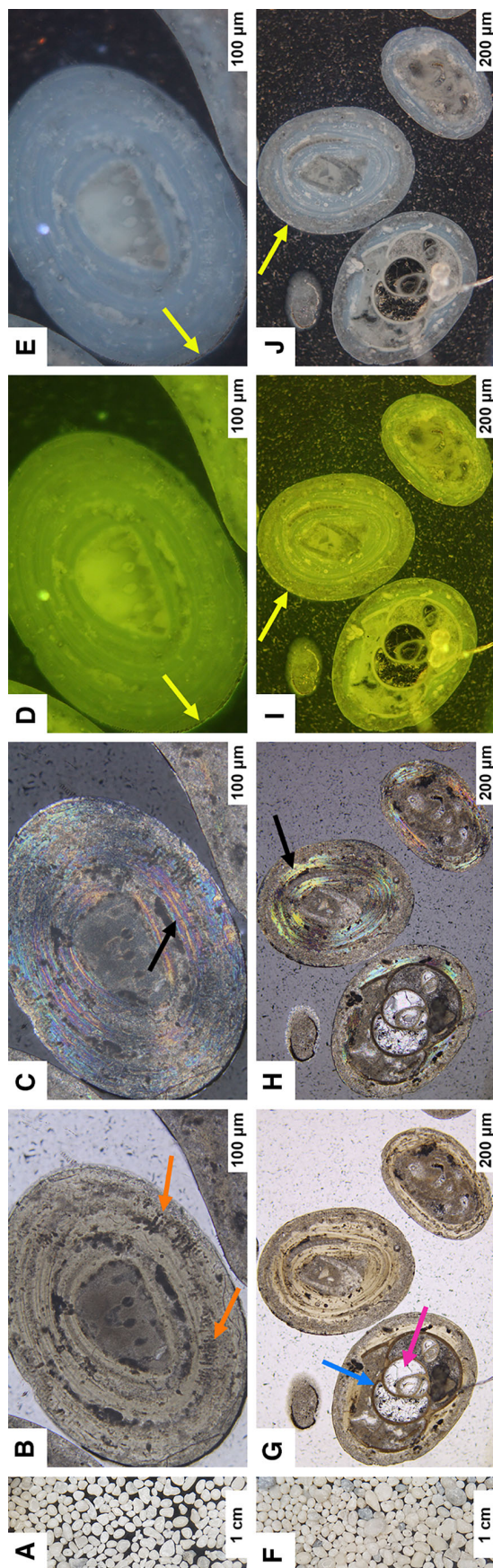


Fig. 2. Reflected and transmitted light microscopic images of Schooner Cays (A) to (E) and Shalil al Ud (F) to (J) ooids, hereafter referred to as GBB (Great Bahama Bank, Schooner Cays) and AD (Abu Dhabi, Shalil al Ud). (A) Binocular microscope image of subsample of ooidal sands from GBB. (B) to (E) Thin section photomicrograph images of an ooid from the GBB sampling site. (B) GBB ooid under transmitted light. Note the prominent vertical microendolithic borings in the cortex (orange arrows) and the <20 cortical laminae. (C) Same as (B), but under polarized light, with non-micritized parts of the cortex showing bright pearlescent colours (black arrow). (D) and (E) Same as (A) and (B) but under fluorescence light. Note the bright fluorescence colours of the unspecified nucleus (mollusc fragment?), and the clearly visible rim cement (yellow arrows). (F) Binocular microscope image of subsample of ooidal sands taken from AD. (G) to (J) Thin section photomicrograph images of various ooids from the AD sampling site. Note nuclei and 4 to 15+, in part micritized, laminae. (G) Transmitted light image showing nuclei (foraminifera, blue arrow, chambers filled with blocky spar, pink arrow) and beige cortex layers. (H) Same as (B) but under crossed polarizers. Note the bright pearlescent colours of non-micritized laminae (black arrow). (I) and (J) Same as (G) and (H) but under fluorescence light. Note the bright fluorescence colours of the biogenic materials (for example, foraminifera) non-micritized layers, and rim cements (yellow arrows).

carbonate grains with diameters between 0.18 mm and 2.0 mm (Fig. 2F).

METHODOLOGY

Fieldwork

Samples were collected during low tide in March 2016 (Shalil al Ud lagoon, Abu Dhabi coastline) and May 2019 (Schooner Cays, Eleuthera Island, Great Bahama Bank; Fig. 1). In both cases, samples were taken from the crests of active ooid shoals.

Sample preparation and analysis

Ooid sand samples (4.5 g ooid sand from Schooner Cays, 7.25 g ooid sand from Shalil al Ud) were sieved using an aggregate shaker (type AS200; Retsch GmbH, Haan, Germany; sieve mesh sizes: 2.0; 1.0; 0.63; 0.5; 0.25; 0.18 mm). The content of each sieve was weighed using a KB 1200–2 scale (Kern & Sohn GmbH, Balingen, Germany). Two petrographic thin sections were

made from unconsolidated ooid subsamples embedded in epoxy resin for each location.

Raman spectroscopy was used in further preparation to determine the mineralogy of ooid cortices and nuclei on a test basis. For a more comprehensive identification of mineralogy, cathodoluminescence microscopy (CL) was used to obtain information on mineralogy throughout the thin section based on characteristic luminescence colours (see Hoffmann *et al.*, 2016; Goldstein *et al.*, 2017). Both methods confirmed that undisturbed ooid cortex layers are usually aragonitic, while cement filling empty boreholes is calcitic. The mineralogy of the nuclei varies according to their composition, but calcitic nuclei predominate (for details, including instrumentation, see Appendix S1–S3).

About 50% of the ooids with a diameter of 0.25 to 0.50 mm were fractured using a mortar. Subsamples (fragments) of ooids from both locations were chemically etched to enhance the ooid microfabrics. The ooids were treated separately with Di-Na-EDTA (0.27 M), HCl (0.1 M) and acetic acid (5 M), with which the ooid sand was soaked for 10 min, 30 min and 60 min; 2 h, 4 h, 6 h and 24 h; and seven days, respectively. After treatment, each ooid subsample was rinsed with distilled H₂O, dried, and mounted onto a sample holder. Overall, 24 ooid samples containing fragmented and etched ooids and 10 samples of untreated ooid sand were investigated. The number of ooid subsamples on a sample holder varied between five to 20 grains/fragments.

The remaining ooids of the size fraction 0.25 to 0.50 mm and those with a size of 0.50 to 0.63 mm were used for the vacuum cast-embedding technique, whereby four casts were made. This technique was applied to visualize the three-dimensional morphology of microborings and assess the penetration depth of the tunnel systems within the ooid cortex. A low-viscosity epoxy resin was used to infiltrate bioerosion features under vacuum conditions. After curing the epoxy resin, the samples were cut to obtain cross-sections of the ooid structure. Subsequently, ooid cross-sections were treated with 5% HCl for 20 s, rinsed with DI water and dried. In an alternative approach, ooids were completely dissolved using 5% HCl, exhibiting the epoxy-filled microborings' positive relief (see Wisshak, 2012, for detailed methodology).

An earlier attempt to identify ichnospecies on etched thin sections did not yield satisfactory

results. However, when used correctly, thin section etching can be a comparatively inexpensive alternative to vacuum casts or for preliminary studies (see Salamon *et al.*, 2019).

Different euendolithic producers create distinct tunnel shapes and sizes, ranging from an assemblage of thin galleries to large solitary tunnels. Specific ichnotaxa were identified by: (i) the appearance of nodular cavities or branching; (ii) the formation of clusters, separate chambers or swellings; as well as (iii) differences in the morphology of tunnel cross-sections or the tunnel terminations and the validity of ichnotaxa was checked back with the annotated list of bioerosion ichnotaxa compiled by Wisshak *et al.* (2019).

Optical techniques

Petrographic thin sections from the different grain size classes of both sampling sites were investigated using transmitted light, crossed polarized light, UV, green and blue epifluorescence. Thin section analysis allowed for the differentiation of grain types and internal structures. Properties such as ooid size, shape and boundaries provide information about the mineralogical composition of a sample and its mode of formation. Structure and composition were described under transmitted light [Olympus BX 51 (Olympus Corporation, Toky, Japan); Leica DM4500P (Leica, Wetzlar, Germany)]. To detect fluorescence patterns in the ooid cortices and nuclei, a Leica DM4500P microscope, equipped with filter cube I3 (excitation filter BP 450–490, dichromatic mirror: 510 nm, suppression filter LP 515) and cube A (excitation filter BP 340–380, dichromatic mirror: 400 nm, suppression filter LP 425) was used. Imaging was performed using a Canon EOS 60D (Canon, Inc., Tokyo, Japan).

The etched ooids were studied under a scanning electron microscope (SEM) Gemini 2 Merlin HR-FESEM (Carl Zeiss AG, Jena, Germany), equipped with a Schottky field emitter serving as an electron source, depicting compositional and topographical properties of the ooids at the nanometre scale. High-resolution images were collected with the E-T and SE in-lens detector under ultrahigh vacuum conditions with an acceleration voltage of 1 to 20 kV and a probe current of 25 to 40 pA. Loose grains were sputter-coated with gold using a Cressington 208HR (Cressington Scientific Instruments, Watford, UK) and thin sections were coated with

carbon using a Quorum Q150T (Quorum Technologies Inc., Puslinch, ON, Canada) to avoid charging effects.

RESULTS

Ooids and ooid fabrics

No systematic differences in shape or size were found when comparing sand grains from the two sampling sites. Ooids display a variety of morphologies ranging from nearly spherical to elongated-ovoid (Fig. 2). Granulometry reveals that the majority of the ooids (>50%) from both locations were 0.25 to 0.5 mm in size. Under the binocular microscope, the ooids appear whitish, light brown or greyish, displaying a dull polished surface. Under transmitted light, ooid cortices are beige to grey with discernible laminae (between three and 45), while ooid nuclei (usually foraminifera, mollusc fragments, unspecified bioclasts or non-carbonate grains) are generally dark-brown (Fig. 2B and G). All ooid cortices show unevenly distributed dark brown or translucent, round-to-tubular patches of varying size and abundance (see Fig. 2B, orange arrows).

Under cross-polarized light, intact ooid cortices display bright pearlescent colours (Fig. 2C and H). Thicker cortices further portray pseudo-uniaxial extinction crosses, with darker bands occurring at the 0°, 90°, 180° and 270° positions, representing the predominantly tangential (c-axis) orientation of the rods, typical for modern marine ooids (Milliman *et al.*, 1974). Epifluorescence reveals successions of darker and lighter shades of green (or blue) for individual cortex layers or a sequence of layers, while micritic areas and peloid nuclei are non-fluorescent or weakly fluorescent (Fig. 2D, E and I to J).

Under the SEM, the surface of ooids comprises batten-like needles, rods and nanograins, with dimensions ranging from 0.1 to 1.0 µm (Figs 3A, 3B, 4A and 4B). Rods and needles are aligned tangentially to the laminae but are oriented randomly within a lamina (Fig. 3B). Besides rods, the ooid cortex also consists of larger, irregular crystallites with a length of 2 to 10 µm (Fig. 3C and D).

Microendolithic borings

Microendolithic borings are present in most of the studied ooid surfaces, but the intensity

of (micro-)bioerosion varies significantly between ooids, independent of the study site. While some grains display only localized features of microendolithic activity, the structural integrity of the surface layer and internal laminae of others is largely destroyed, and the cortical layers are obliterated (Fig. 3E and F). Carbonate cements on bioerosion cavity walls (Fig. 3G) exhibit a broad spectrum of morphologies. The most common are fibrous, acicular, or needle-shaped cement (Fig. 3H). Less commonly, columnar morphologies are present. Extracellular polymeric substances (EPS) of microbial origins are observed in the vicinity of bioerosion features at the ooid surface and the cortex layers (Fig. 4). The EPS-biofilm appears as smooth layers covering substantial portions of the ooid surface and occurs as long strands or torn filaments stretching between rods or crystals (Fig. 4A to F). Desiccated remnants of microbial EPS commonly extend between cavity walls. Rods or nanograins are prevalent within or on the EPS surface or occur in clusters at the margins of biofilm layers (Fig. 4A and D). Rods appear to preferentially form in net-like structures that resemble honeycomb or alveolar sacs. Various microbial organisms and collapsed microbial sheaths occur in bioerosion cavities, commonly in direct proximity to EPS. These include (in descending order of abundance) various genera of diatoms, cyanobacteria, coccolithophores and unidentified bacilli bacteria (Fig. 4C and F to H).

Observations of the vacuum casts reveal a range of microbioerosion traces (referred to as ichnotaxa) in cortical layers, characterized by distinctive sizes and shapes (Fig. 5). Microborings are most accessible in the outer cortex, particularly due to numerous open borings (Fig. 5A to C). Most microborings have a tubular to vermiform shape with distinct constrictions (Fig. 5D to F). For practical purposes, borings can be roughly separated into three categories based on diameter sizes: (i) small (*ca* <5 µm); (ii) intermediate (*ca* 5 to 15 µm); and (iii) large (>15 µm). Borings appear as single horizontal or vertical strings in larger clusters or wide galleries. Some ooids display super-surficial but extensive fan-shaped bioerosional features (cf. Fig. 5B).

Single microbioerosion traces extend into the ooid cortex and nucleus as much as 50 µm. Ooid nuclei show distinct patterns of microborings. Multiple ichnotaxa are generally present in a single ooid, resulting in a rather irregular

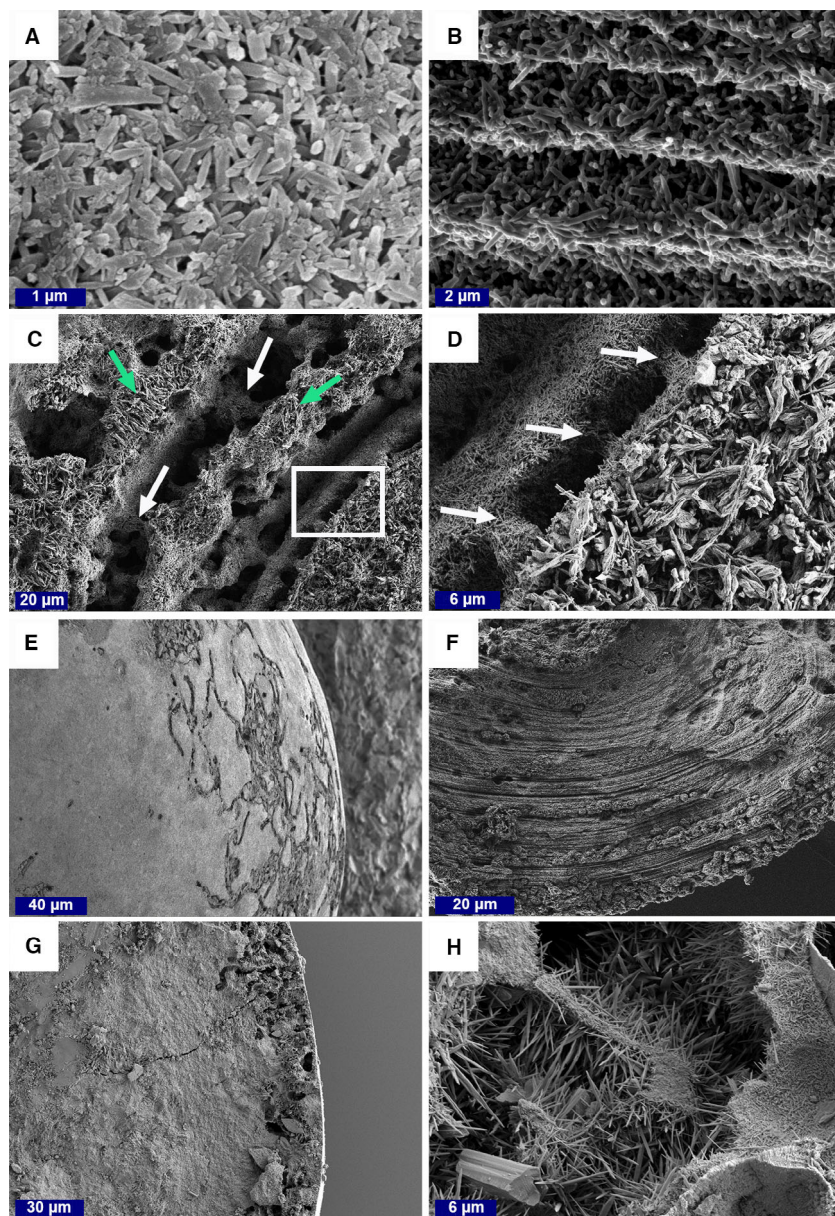


Fig. 3. Scanning electron microscopy (SEM) images of distinct features and microbioerosion traces in marine ooids, accentuated by etching agents – Great Bahama Bank (GBB): A, E, F, G, H; Abu Dhabi (AD): B, C, D. (A) Magnification of an ooid surface. Note the combination of rods, nanograins and cement forming the solid surface. (B) Cortical layers (etched with 0.1 M HCl, 6 h). Note the random orientation of rods between horizontally arranged planes with a much denser packing of rods. (C) and (D) Vertical bridges of randomly orientated rods (white arrows) connecting cortical layers (5 M acetic acid, 30 min). Note the larger crystallites, attributed to microendolithic bore traces, which accumulate on top of or in between finer rods (green arrows). (E) Ramified network of microendolithic borings disrupting an ooid surface. (F) Sequential changes of nearly undisturbed cortical layers and intervals of heavy microendolithic reworking (etched with 0.27 M EDTA, 1 h). (G) Cavities beneath the outer surface. Older borings closer to the nucleus are filled with carbonate. (H) Aragonite needles developing in surficial cavities.

distribution of cortical microborings (Fig. 5B). Irregular clusters of small (*ca* 1 µm in diameter) round to oval tunnels and galleries are found close to tubular borings. Thin strings, lacking constrictions (<1 µm in diameter), can be observed crossing or overlaying larger (>1 µm) ichnotaxa (Fig. 5G and H).

The SEM analysis on the vacuum casting samples reveals that ooids from both localities harbour a diverse assemblage of ichnotaxa, mainly represented by a total of 12 ichnogenera (Table 1; Fig. 6). Table 1 lists concise information about ichnotaxa inferences, characteristic features and environmental implications.

INTERPRETATION AND DISCUSSION

Ooid microfibrils and microborer activity

Mechanical abrasion in agitated depositional settings dictates the orientation of rods of the outermost ooid cortex layers, and leads to polishing and compaction of the ooid surface. The ooid surface is prone to bioerosion caused by microbial organisms such as cyanobacteria, algae or fungi, for example, microendoliths, that chemically dissolve the outmost cortex layer.

Microborers leave shallow, horizontal or vertical tunnels in the surface layers. The latter

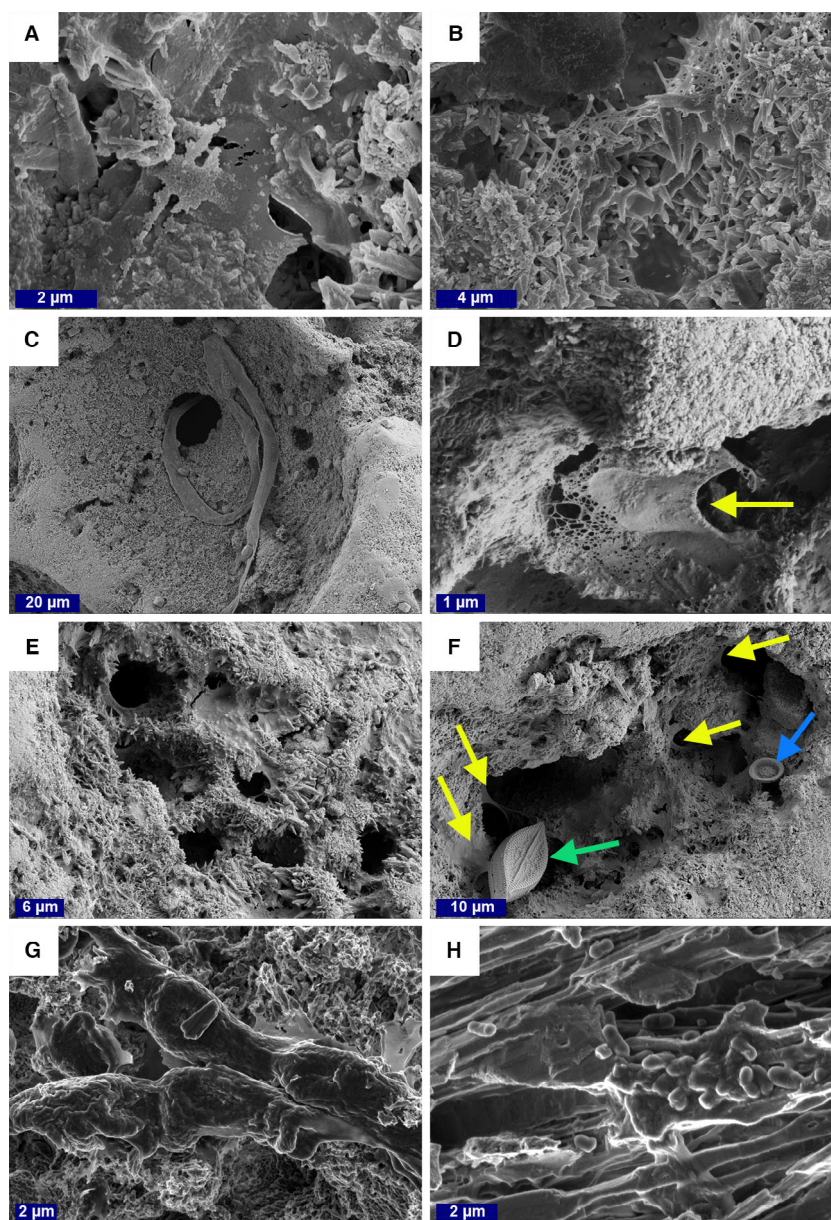


Fig. 4. Scanning electron microscopy (SEM) images of biofilms and microbes on marine ooids – Great Bahama Bank (GBB); A–D, G–H; Abu Dhabi (AD): E, F. (A) Extracellular polymeric substance (EPS) biofilm blanket with amorphous calcium carbonate (ACC) and strands extending over and between ooid surface irregularities (cement, boreholes). (B) Thin reticulate EPS strands stretching between single rods. (C) Collapsed microbial filament protruding from a vertical borehole. (D) Biofilm blanket covering a cavity. The marginal thickening (yellow arrow) and the graininess (blue arrow) in the centre of the blanket indicate the nucleation of ACC. (E) EPS, rods and larger acicular crystals forming honeycomb-like structures. (F) Variety of microbial life (for example, pennate diatom, green arrow; coccolith, blue arrow) in direct proximity to EPS (yellow arrows) inside surface cavities. (G) Microbial filament surrounded by desiccated EPS. (H) Coccobacillus bacteria, characterized by short rods and oval shape morphology.

suggests reworking of the underlying fabric with extensive tubular boring networks and developing widespread subsurface voids that likely compromise the ooid's structural integrity and resistance to physical abrasion. This could result in cavity collapse due to ooid transport and collision with other ooids. The collapse of these cavities results in the formation of irregular pits at the ooid surface. The partial loss of the hard ooid surface leads to increased microbial colonization of internal cortical layers, because the microendolithic communities can penetrate deeper into the ooid and become protected from both mechanical abrasion and predators.

Sequences of cortical layers with varying degrees of microborings and micritization, i.e. intact versus bored and micritized layers, point to the alternation of periods with undisturbed (or less disturbed) ooid cortex growth ('colonization window') followed by periods with a microbial reworking of the outer layers. This results in competition between eroders and constructors at the ooid surface, with the development of irregular cement crystals precipitating in open borings and cavities. The secondary precipitates develop after the rods have formed but in their immediate vicinity. Still, it remains uncertain whether the same microorganisms responsible

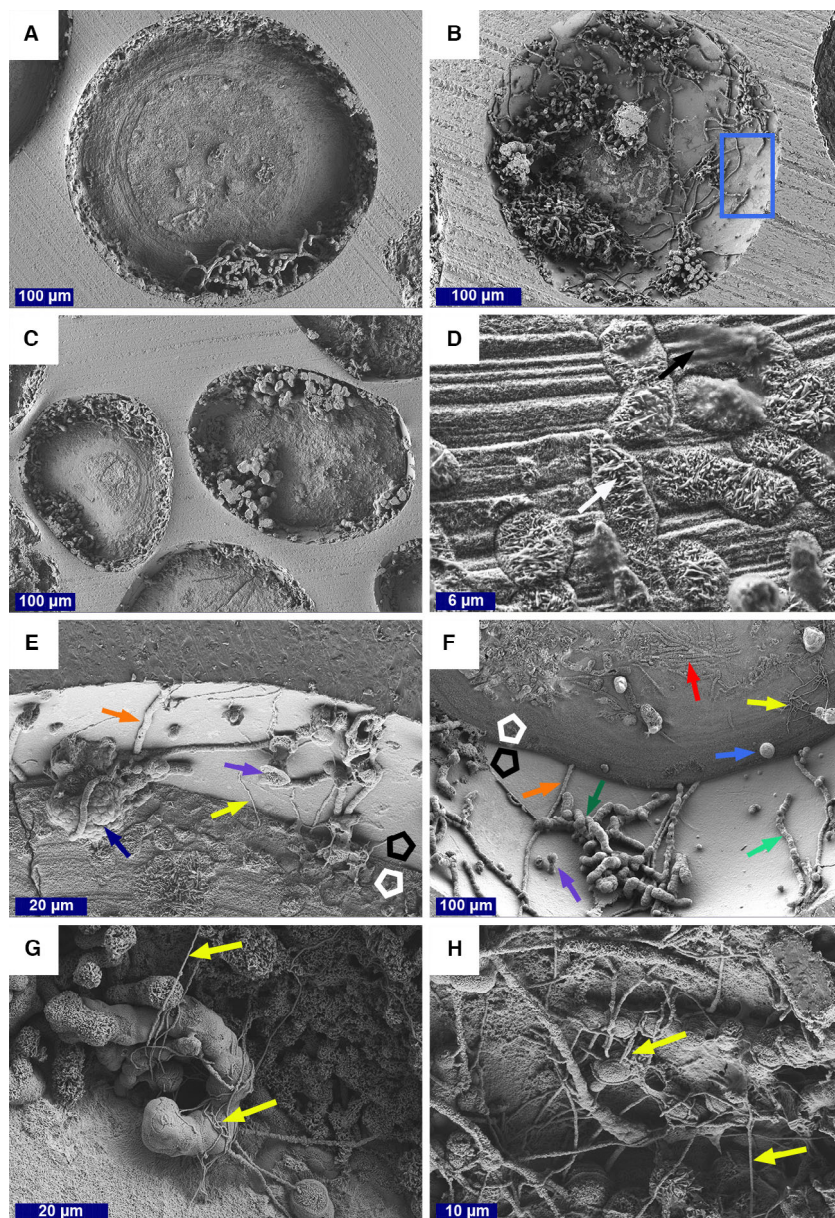


Fig. 5. Scanning electron microscopy (SEM) images of endocasts of different ichnotaxa in the ooid cortex – Great Bahama Bank (GBB): A, C, E, G; Abu Dhabi (AD): B, D, F. (A) Average ooid showing the common extent of microendolithic damage to the cortex. (B) Inhomogeneous distribution of the microboring pattern. Note the differentiation between horizontal tubes and cauliflower-like domes. Note also the superficial fan-shaped bioerosion traces (blue rectangle). (C) Dimensional difference between ichnotaxa (left ooid = medium; right = large). (D) Filled vertical microborings (white arrow) and preparation residues (black arrow) in an ooid cortex. Note the dimensional difference between the layer forming rods and the needle to plate cement filling the boreholes. (E) and (F) Various ichnotaxa marked by arrows. Orange: tubular strings without constrictions; purple: vertical borings; red: filled bore traces in the ooid cortex; dark green: cluster of tubular tunnels, light green: string tubular tunnels; light blue: roundish features with a smooth surface; dark blue: nodular roundish features; yellow: threads attached to larger features. The black polygon indicates the surface of the ooid, while the white polygon marks the ooid cross-section. (G) and (H) Narrow threads (yellow arrows) overlying other (larger) ichnotaxa, indicating episodic occurrence of different producers.

for cortex destruction are also (indirectly) responsible for rod and cortex generation.

Furthermore, it cannot be completely ruled out that biofilms excreted by different producers would not also lead to the formation of variable secondary precipitates. Some hypotheses abound seeking to explain this geochemical paradox, whereas concurrent physiological activities (i.e. photosynthesis and respiration) of endolithic cyanobacteria are an antagonistic effect, thereby promoting both calcification and bioerosion of the substrate (see McCutcheon *et al.*, 2016). While some attribute this dichotomy to a temporal and/or spatial separation of photosynthesis and boring

activities – triggering the production of alkali and acid metabolites (Macintyre *et al.*, 2000; Reid & Macintyre, 2000) – others propose a mechanism based on the active transport of Ca^{2+} ions via calcium pumps (Garcia-Pichel *et al.*, 2010).

Ichnotaxa and their corresponding light dependence in shallow waters and the uppermost sediment column

The observed microendolithic traces can be attributed to cyanobacteria (photoautotrophic organisms), with *Fascichnus frutex*, *F. dactylus*, *F. rokus*, *Eurygonum nodosum* and *Scolecia*

Table 1. Overview of occurring ichnotaxa, including characteristic features, inferred producers and environmental implications. AD: Abu Dhabi, GBB: Bahamas, OM: organic matter, X: present, (X): uncertain, \varnothing : diameter, L, length. The ichnotaxa are sorted after their respective ichnofamilies (see Wisshak *et al.*, 2019).

Ichnotaxon	AD	GBB	Characteristics	Inferred producer (Biotaxon)	(Palaeo-)environmental indications
<i>Fascichnus acinosus</i> (Glaub, 1994)	X		Nodular cavities (\varnothing 5–10 μm ; L: ca 80), often clustered together	Cyanobacteria (<i>Hyella balani</i>)	Common in euphotic zone; intertidal
<i>Fascichnus dactylus</i> (Radtko, 1991)	X	X	Thin galleries/clusters with uniform diameters (\varnothing 4–8 μm) and rare bifurcations	Cyanobacteria (<i>Hyella caespitosa</i> , <i>Hyella</i> sp., <i>Solentia</i> sp.)	Intertidal to subtidal; common in shallow euphotic zone, rare in deep euphotic zone
<i>Fascichnus frutex</i> (Radtko, 1991)	X	X	Galleries (\varnothing 8–15 μm), common bifurcations and cell-like constrictions, round and blunt terminations	Cyanobacteria (? <i>Hyella gigas</i>)	Common in shallow euphotic zone, rare in deep euphotic zone
<i>Fascichnus rognus</i> (Bundschuh & Balog, 2000)	X	X	Cauliflower-shaped colonies (\varnothing 50–90 μm) with densely spaced to fused radiating galleries; rounded terminations (\varnothing 4–6 μm)	Cyanobacteria (<i>Hyella racemus</i> , ? <i>Hyella conferta</i>)	Shallow euphotic
<i>Eurygonum nodosum</i> (Schmidt, 1992)	X	X	\varnothing 4–6 μm , dichotomous branching, lateral nodular swellings (\varnothing 4–8 μm), round to blunt terminations, common bifurcations	Cyanobacteria (<i>Mastigocoleus testarum</i>)	Common in shallow euphotic zone, rare in deep euphotic zone; indicating high levels of (inorganic) nutrients
<i>Scolecia fibose</i> (Radtko, 1991)	X	X	Thin, uniform galleries (\varnothing 1–2 μm ; L: >100 μm), rare bifurcations, commonly overlying other traces	Cyanobacteria (<i>Plectonema terebrans</i>)	Common in shallow-euphotic to deep euphotic zone, rare in dysphotic zone; indicating high levels of OM + nutrients
<i>Cavernula pediculata</i> (Radtko, 1991)	X	(X)	Solitary and large borings (\varnothing 20–35 μm ; L: 30–70 μm), irregular cavities, dome-shaped, occasional rhizoidal appendages, commonly perpendicular to ooid surface	Chlorophyta (? <i>Gomontia polyrhiza</i>)	Common in shallow-euphotic zone; in high latitude settings as substitute for <i>Fascichnus acinosus</i>
<i>Ichnoreticulina elegans</i> (Radtko, 1991)	(X)		Reticulate networks of thin (\varnothing ca 3 μm) galleries, substrate parallel, flattened (oval) cross-sections	Chlorophyta (<i>Ostreobium quekettii</i>)	Common in shallow-euphotic to deep euphotic zone, rare in dysphotic zone
<i>Planobola macrogota</i> (Schmidt, 1992)	X	X	Spherical to semi-spherical cavities, \varnothing 15–60 μm , lateral substrate contact	?cyanobacteria, ?chlorophytes, ?fungi	Shallow euphotic zone

Table 1. (continued)

Ichnotaxon	AD	GBB	Characteristics	Inferred producer (Biotaxon)	(Palaeo-)environmental indications
<i>Orthogonium lineare</i> (Glaub, 1994)	(X)	X	Thin galleries of tubular borings (ø 5–15 µm), parallel to ooid surface, perpendicular branching	Organotrophs (?fungi)	Common in dysphotic to aphotic zones, rare in shallow euphotic to deep euphotic zone
<i>Saccomorpha clava</i> (Radtko, 1991)	(X)		Club-shaped to sack-shaped (sporangial) borings (L: 10–12 µm), thin interconnecting substrate-parallel (hyphal) galleries	Fungi (<i>Dodgella prisca</i>)	Common in dysphotic to aphotic zones, rare in shallow euphotic to deep euphotic zone; indicating high levels of OM
<i>Saccomorpha sphaerula</i> (Radtko, 1991)	X		Small spherical (sporangial) chambers interconnected by thin (hyphal) galleries	Fungi (<i>Lithopythium gangliiforme</i>)	Common in shallow euphotic zone, rare in deep euphotic zone
Chambered tunnels (undefined trace)	X	X	Flat intercalary or lateral chambers (ø 10–15 µm) connected by nodular, often perpendicular branching tunnels (ø 3–5), round terminations	?	?

filosa being the most abundant ichnotaxa in the ooids from both locations studied (see Table 1; Fig. 6). The study presented here confirms previous work (e.g. Harris *et al.*, 1979; Gektidis, 1997; Gektidis *et al.*, 2007; Radtko & Golubic, 2011).

Microendoliths are attributed to the benthic community and are most active at the sediment–water interface and inside the shallow sediment column (see May & Perkins, 1979; Golubic *et al.*, 1984). Since distinct euendolithic taxa are known to have specific low-light tolerances and light optima, information about the relative bathymetry and ecology for ooid cortex formation can be obtained by noting the presence or absence of their respective index ichnotaxa by allocating the inferred index producer to the euphotic (>1% surface illumination), dysphotic (0.01 to 1% surface illumination; respiration rates exceed photosynthesis rates), or aphotic (<0.01% surface illumination; inhibited photosynthesis) zone (see del Giorgio & Peters, 1994; Glaub, 1994; Glaub *et al.*, 2001, 2007; Wisshak, 2012).

In the supratidal and intertidal zones, cyanobacteria generally dominate. In the shallow subtidal zone, these organisms are joined by septate chlorophytes (Glaub *et al.*, 2007). As an example, the ichnotaxon *Ichnoreticulina elegans*, produced by the siphonal green alga *Ostreobium quekettii* and other species in that genus, and *Scolecia filosa* produced by the cyanobacterium *Plectonema terebrans*, are attributed to the dysphotic zone, while heterotrophic organisms (for example, fungi such as *Dodgella prisca*), which are independent of light exposure, generally occur in the aphotic zone and are prominently represented by *Saccomorpha clava*, a key ichnotaxon of the aphotic index microboring ichnocoenosis (Glaub, 1994; Försterra *et al.*, 2005; Glaub *et al.*, 2007, see Table 1).

Particle size and composition determine light penetration in the uppermost portion of the sediment column (Colijn & de Jonge, 1984; Sullivan & Moncreiff, 1988; Pinckney & Zingmark, 1993). The abundance and vertical distribution of benthic biomass, for example, microalgae in sediments, depends on factors such as temperature, resuspension, nutrient and light availability, salinity, pH, desiccation, grazing and bioturbation (e.g. Cartaxana *et al.*, 2006; Ichimi *et al.*, 2008; Wisshak, 2012). Fenchel & Straarup (1971) noted a rapid decrease in irradiance to 50% at a sediment depth of 0.65 mm for particle sizes of up to 1 mm (see Ichimi *et al.*, 2008). Generally, the larger the sediment particles, the deeper the light penetrates the uppermost sediment column

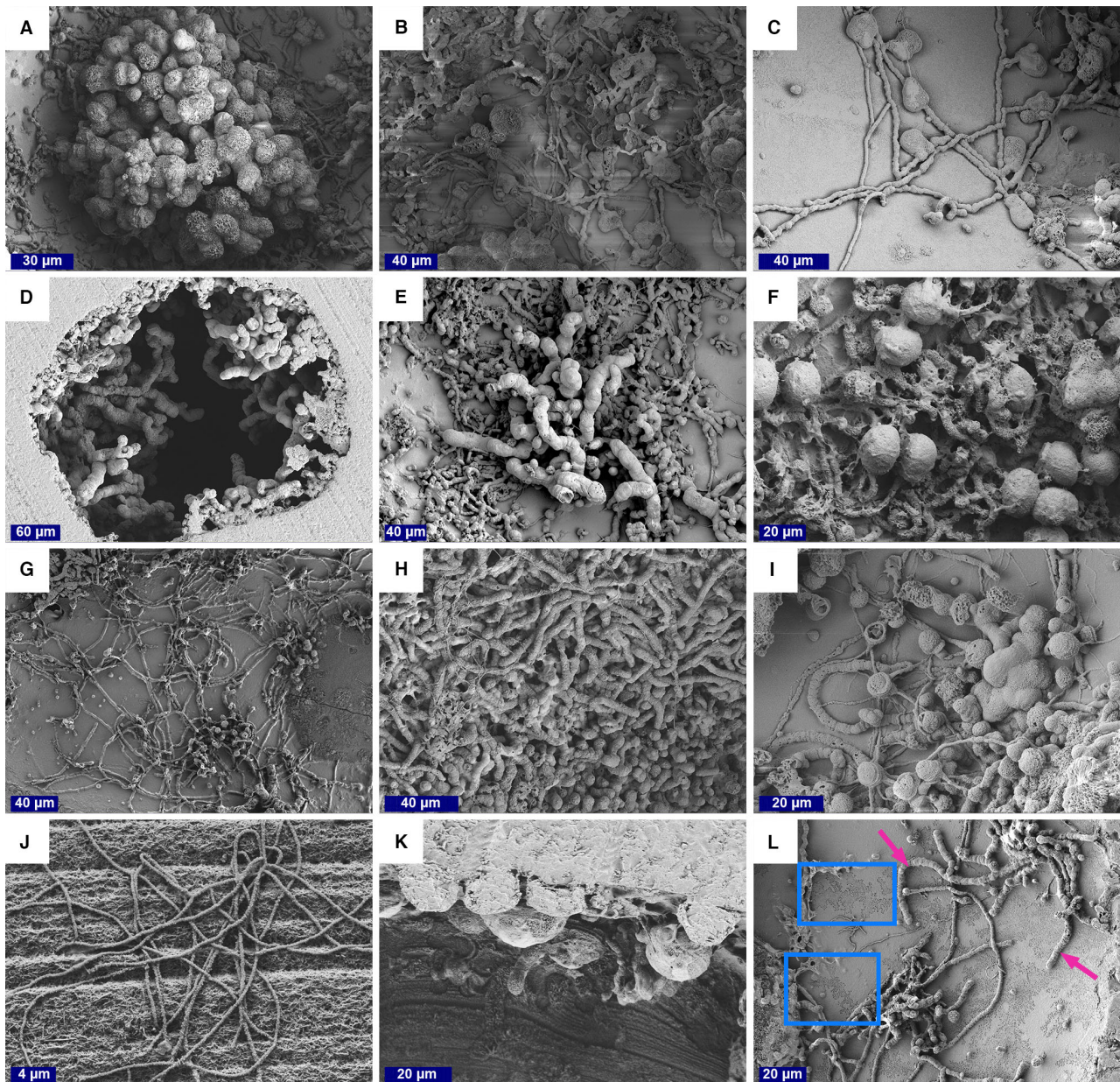


Fig. 6. Scanning electron microscopy (SEM) images of selected ichnotaxa from Schooner Cays (GBB) (A) to (F) and Shalil al Ud (AD) shoals (G) to (L). (A) *Fascichnus rogus* (large). (B) and (C) Previously unknown morphology with intercalar and lateral flat chambers. (D) and (E) *Fascichnus frutex*. (F) *Cavernula pediculata*. (G) *Orthogonum lineare* (though very thin). (H) Collapsed *Fascichnus ?dactylus*. (I) *Saccomorpha sphaerula* (left). (J) *Scolecia filose*. (K) *Planobola macrogota*. (L) *Eurygonum nodosum* (pink arrow, note the fan shaped super surficial bioerosion features, blue rectangles).

(Gomiou, 1967; Kühl *et al.*, 1994; Yallop *et al.*, 1994). Given the ooid size of ≤ 2 mm at the formation sites, an abundance of larger particles (for example, shell fragments), and reflective or even partly translucent grain surfaces, it is inferred that the depth at which light intensity is reduced by 50%, is deeper than 0.65 mm and may reach

down to several centimetres (see Gomiou, 1967). At the studied sites, turbulent currents result in ooids experiencing periods of burial to various depths, either within ooid shoals or intershoal domains, punctuated by episodes of resuspension and transportation at the sediment surface over a time of minutes to hours.

This is relevant because it implies that while the ichnocoenosis of a given ooid in the water column or at the sediment surface may correspond to the shallow euphotic zone, the ichnocoenosis, when buried deep enough, may shift towards one that is typical of the dysphotic to aphotic zone, with only the upper limit of the aphotic zone defined. For clarification, a given ooid buried at depths of approximately >30 cm to >1 m below the ooid shoal seafloor may be infested by microorganisms typical for the aphotic zone. This implies that microendolithic ichnotaxa can be applied as a proxy for ooid burial depth, even though both the Schooner Cays and the Shalil al Ud lagoon are characterized by an intertidal to shallow subtidal setting and clear water conditions. The studied ooid shoals are exposed during low tide and flooded during high tide. Intershoal domains are, depending on the location considered, in the shallow subtidal range, but intershoal channels of some metres of water depth also occur.

Consequently, the terms euphotic, dysphotic and aphotic, as used in the classical subdivision based on the light penetration depth of the water column (see Glaub *et al.*, 2001, 2007; Wisshak *et al.*, 2011), are not fully applicable in this context and have instead been substituted by light penetration levels (Levels 1 to 3, see Fig. 7).

Level 1 corresponds to the area between the sea surface and the immediate vicinity of the seafloor at a depth with approximately 1% of surface light (Glaub *et al.*, 2001; see Wisshak, 2012). It refers to a region where the ooids are suspended in the water column and are exposed to high levels of illumination, and is characterized by euendolithic organisms usually attributed to the shallow euphotic realm (shallow I–II). *Level 2* refers to an area where the ooid periodically resides within the uppermost region of the sediment column but not for an extended period, as the ooid may be exhumed due to wave and tidal activity. It is characterized by euendoliths in the euphotic to deep euphotic zone. *Level 3* refers to a region where the ooid is buried within the sediment pile at, relatively speaking, greater depth. There it can no longer be resurfaced by the diurnal tide and average wave action and therefore remains idle for a prolonged period. Level 3 is characterized by euendoliths that prevail in the dysphotic to aphotic zone (see Fig. 7).

Depending on how long the ooid remains in one of these levels, the number of

(cyanobacterial) borings in the ooid cortex and their resultant orientation will vary. Given that many euendolithic cyanobacteria are excellent palaeodepth indicators as they are stenobathic, showing a limited vertical distribution restricted to a narrow depth range (Glaub *et al.*, 2001), it is possible to connect the orientation of borings to the proposed light penetration zones.

While vertical borings seem the most common in Level 1 (corresponding to the intertidal zone), horizontal borings are more typical in Level 2 (corresponding to the subtidal zone, see review in Glaub *et al.*, 2001; Wisshak, 2012).

Based on these findings, the migration of ooids between different light penetration zones in the shallow marine realm derived from the form and orientation of cyanobacterial borings can be linked to different stages in ooid cortex growth, including an agitation stage, a resting stage, a sleeping stage and a reactivation stage (cf. Davies *et al.*, 1978; Duguid *et al.*, 2010; Anderson *et al.*, 2020).

Relation of oxic–anoxic zonation of ooid cortices with bioeroder distribution

Ooids can be considered as mini bioreactor sedimentary systems in which the outside is akin to the sediment surface where diagenetic processes are dominated by aerobic processes, and layers further into the centre of the ooid represent areas further removed and experiencing more anoxic regimes dominated by bacterial nitrate and sulphate reduction (Fig. 8). Evidence of these geochemical processes was provided not only by genetic analyses (Diaz *et al.*, 2013a, 2013b) but also by the isolation of remnants of these geochemical reactions, such as elevated nitrate concentrations and $\delta^{15}\text{N}$ values and lower $\text{SO}_4^{2-}/\text{Cl}^-$ ratios (Diaz *et al.*, 2015). As these processes proceed, diffusion gradients become established, with ions diffusing into and out of the ooid, supplying and removing reactants. Such zones may not always be consistent in their location because the ooids may be buried in a zone where the external environment might favour the development of more anoxic microenvironments within the ooid cortex, and gradients may be reversed. Such diagenetic processes then may be mirrored by the infestation by the endolithic organisms, with photosynthetic biota occupying the zones characterized by aerobic processes, while fungi and anaerobic biota, including anoxygenic phototrophs (for example, green sulphur bacteria, purple bacteria

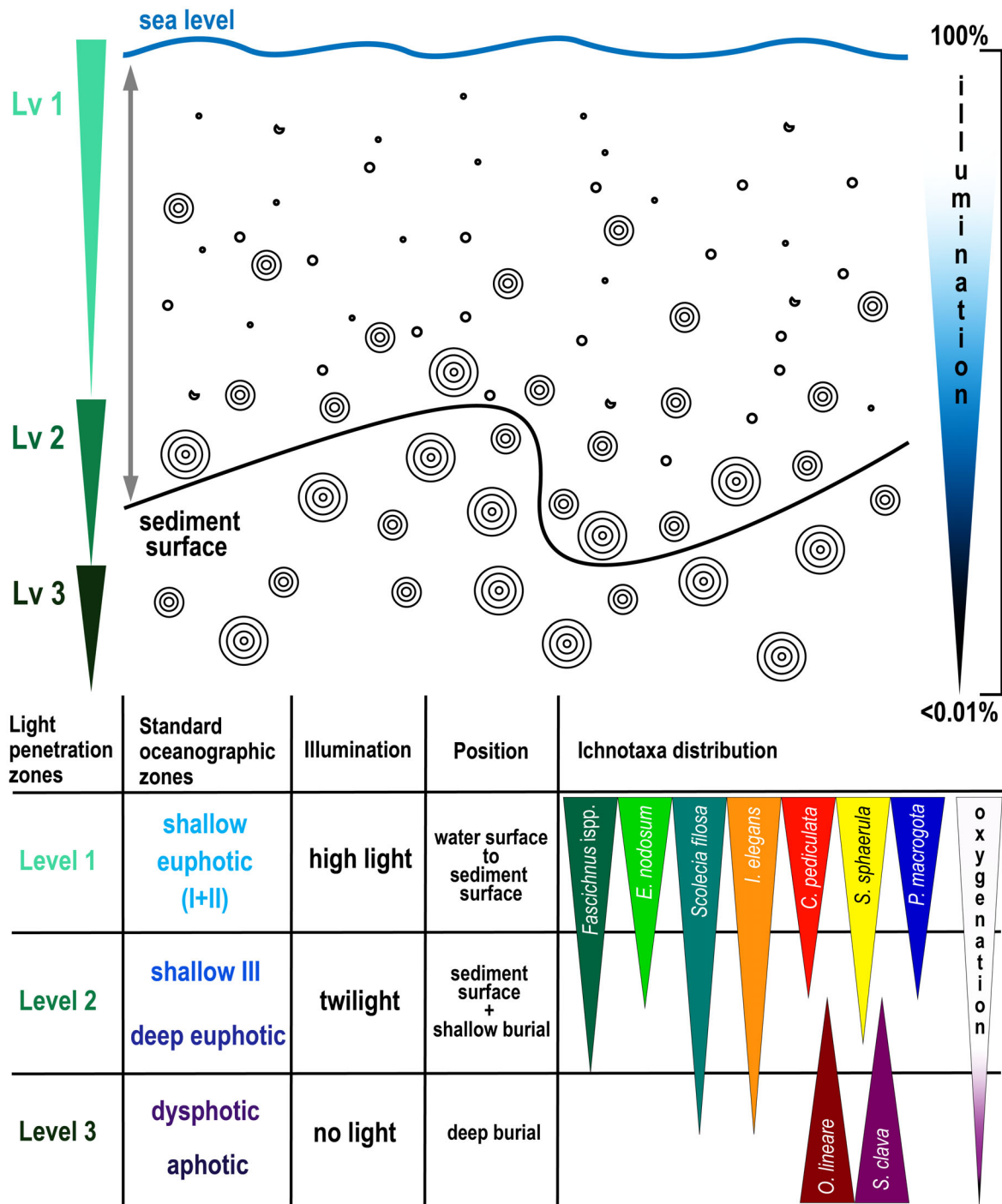


Fig. 7. Division of light penetration zones (Levels) based on euendolithic occurrence. Level 1 (high light zone) marks the area between the sea surface and the very top of the sand dunes. At Level 1, traces of photosynthesizers prevail, so that a parallel can be drawn to the range of the shallow euphotic realm (shallow I + II) of the standard oceanographic zones. Level 2 (twilight zone) marks an area ranging from between the sand dunes to shallow burial. The illumination at Level 2 is highly fluctuating so that this level was equated to the shallow III to deep euphotic zone. Level 3 (no light zone) marks an episode of deep burial with no illumination. Based on the ichnotaxa found (suboxic chemotrophs and fungi), Level 3 was set as a synonym to the dysphotic to aphotic realm. The degree of light transmission in the sediment pile depends on the grain size (Kühl *et al.*, 1994; Yallop *et al.*, 1994). The residence time in the different zones depends mainly on wind and wave action, and tidal currents.

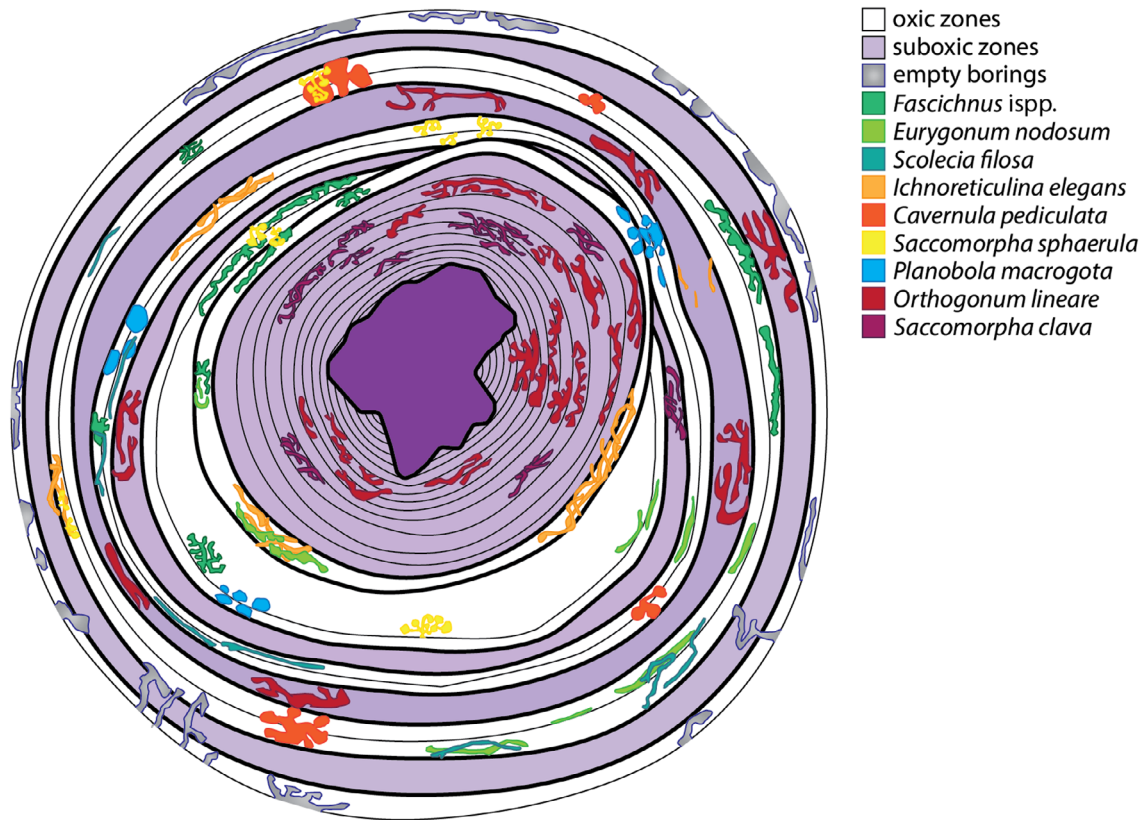


Fig. 8. The sketch of an ooid illustrates the relationship between oxic (white) and anoxic (purple) zones and their associated ichnotaxa, which is indicated by a colour code. Note that not all discovered borehole features could be assigned to a particular ichnotaxon, and some of the ichnotaxa were likely not discovered. The colour code for the different ichnotaxa is shown in the upper right and was also used for the ichnotaxa distribution in Fig. 7. Most traces in the oxic zones are attributed to cyanobacteria (various *Fascichnus* species, *Eurygonum nodosum* and *Scolecia filosa*) followed by chlorophytes (*Ichnoreticulina elegans*, *Cavernula pediculata*) and rare fungi (*Saccomorpha sphaerula*). The suboxic regime is characterized by chemotrophs (for example, *Orthogonum lineare*) and fungi (for example, *Saccomorpha clava*). The producer is unknown in some cases (for example, *Planobola macrogota*).

and Chloroflexi) primarily colonize anoxic or microaerophilic areas on the grain.

Ooid formation model based on agitation, resting and sleeping stages

The following relationship between ooid formation stages and microbial interaction at Level 1 (high light), Level 2 (twilight) and Level 3 (no light) is proposed (Fig. 9).

Agitation/suspension stage – Level 1, corresponding to shallow euphotic zone I–II

This stage is situated at the interface between the water column and the seafloor, i.e. at the surface of the ooid shoal. Cyanobacteria and other microbes colonize the surface of carbonate (i.e.

skeletal fragments) and non-carbonate particles (i.e. faecal pellets and quartz) that later become the ooid nuclei. As colonization takes place, microbial exudates surround the nuclei, forming an EPS-biofilm that – upon degradation – acts as locations for the initial steps of crystal nucleation through the amorphous calcium carbonate (ACC) phase (Duguid *et al.*, 2010; Diaz *et al.*, 2017). As aggregates of ACC form, secondary nucleation promotes the formation of the first cortical layer comprising aragonite needles. During this stage, ooids are constantly agitated due to wave and current activity, moving freely in the water column and at the shoal surface. Rolling and saltation at the sediment surface and collision with other grains result in the flattening (tamping down) of newly formed and randomly orientated aragonite

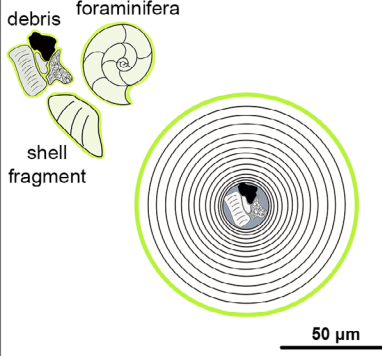
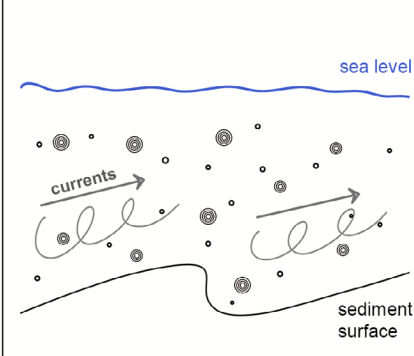
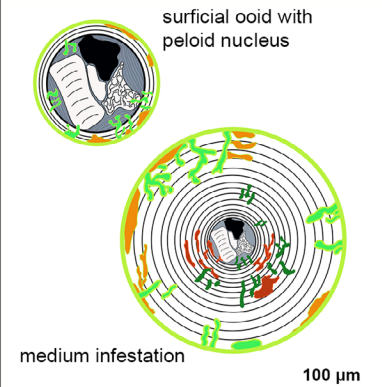
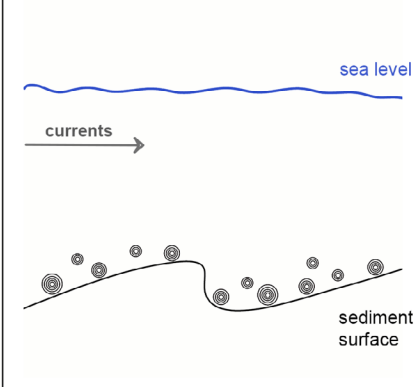
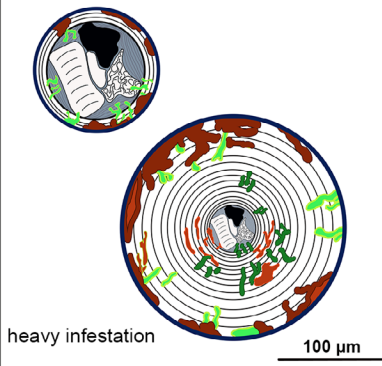
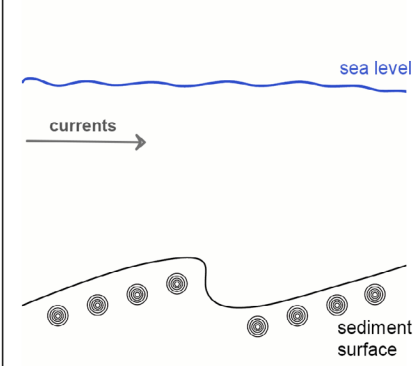
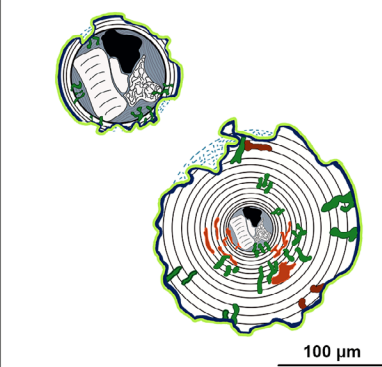
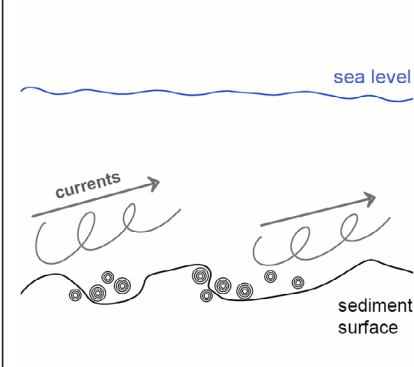
	Explanation	Biofilm / microborer activity	Environment
1. Agitation Stage	<p>Extrapolymetric substance</p> <ul style="list-style-type: none"> → Agglutinated debris and shell fragments serve as nuclei → Nucleation of ACC from EPS-biofilm template → Little to no colonization by euendoliths 	<p>debris foraminifera</p> <p>shell fragment</p>  <p>50 μm</p>	<p>sea level</p>  <p>currents</p> <p>sediment surface</p>
2. Resting Stage	<p>Empty vertical / horizontal borings</p> <p>Filled vertical / horizontal borings</p> <ul style="list-style-type: none"> → Colonization by boring organisms in two subphases: first vertical, then horizontal traces → Polished/hard surface due to agitation → Continuous biofilm production / ACC nucleation 	<p>surficial ooid with peloid nucleus</p> <p>medium infestation</p>  <p>100 μm</p>	<p>sea level</p>  <p>currents</p> <p>sediment surface</p>
3. Sleeping Stage	<p>Pervasive bioperforation</p> <ul style="list-style-type: none"> → Colonization of the surface and preceding borings → Filling of older bore traces → Presumably longest stage 	 <p>heavy infestation</p> <p>100 μm</p>	<p>sea level</p>  <p>currents</p> <p>sediment surface</p>
4. Reactivation Stage	<p>Infilling of pits with rods and carbonate cements</p> <ul style="list-style-type: none"> → Shift in microendolithic community → Restart of biofilm production and ACC nucleation → Transition to active stage 	 <p>100 μm</p>	<p>sea level</p>  <p>currents</p> <p>sediment surface</p>

Fig. 9. Modern ooid growth and cortex infestation model (after Davies *et al.*, 1978, and Anderson *et al.*, 2020, with respect to the results of Duguid *et al.*, 2010, and Diaz *et al.*, 2017). The four different stages of ooid cortex growth include an agitation stage at Level 1, characterized by very little microboring activity and the formation of amorphous calcium carbonate (ACC) nucleating from extrapolymeric substance (EPS) biofilms on the grain surface; a resting stage at Level 2, characterized by an increased physical abrasion and microborers; a sleeping stage at Level 3, characterized by burial in the sediment with not light and strong bioperforation of the cortical layers; and a reactivation stage where the ooids are resurfaced to Levels 1 and 2, and subsequently characterized by a shift in the microbial community from heterotrophs (mainly fungi) to photosynthesizers. While aerobic processes prevail in the outmost cortex layers, suboxic conditions can develop in microenvironments in deeper cortex layers due to bacterial nitrate and sulphate reduction. Anaerobic processes take place predominantly during the sleeping stage, favoured by the absence of light and the generally lower oxygen supply.

needles. This results in tangential crystal orientation of the needles and polishing and compaction of the cortex layer that forms the ooid surface. The presence of cyanobacteria produces mainly vertical tunnels. At this stage, microendolithic communities are influenced by both photic and hydrodynamic factors (Glaub *et al.*, 2001) and chlorophyte colonization of the ooid surfaces is strongly limited due to constant movement and mechanical erosion of the ooids (Gektidis, 1997).

Resting stage – Level 2, corresponding to shallow III to deep euphotic

Temporary burial of the ooid in the uppermost shoal or intershoal setting impedes ooid growth (Gektidis, 1997; Diaz *et al.*, 2017; Anderson *et al.*, 2020). The immobilization of ooids leads to colonizing cortices by microorganisms preferring stable environmental conditions. Euendolithic assemblages change their composition and boring behaviour (Glaub *et al.*, 2001). In contrast to the shallow I and II zones, here, horizontal boring patterns dominate as a result of decreased illumination, possibly indicating the initiation of a shift from phototrophic to heterotrophic organisms. Based on the ichnotaxa analysis of the casts, the main microbial colonizers in the ooid cortices continue to be cyanobacteria, accompanied by increasing numbers of chlorophytes, rhodophytes and fungi.

Sleeping stage – Level 3, corresponding to dysphotic to aphotic

The ooid is buried in the upper sediment column (centimetres to a few metres) of the ooid shoal for an extended period, and no sunlight penetrates to this depth. Nevertheless, this stage is characterized by increased microbial bioerosion. Numerous but shallow borings with a horizontal orientation occur. The crystallization of ACC to aragonite needles continues. Moreover, direct carbonate precipitation from porewater, in

combination with microbial interactions, is likely. Bore traces are partially occluded with carbonate cement crystals. Microbial fingerprints on the casts identify heterotrophs (i.e. fungi) dominating the microborer spectrum. The abundance of organotrophs is expected to rise with burial depth. Photosynthesizing organisms are absent due to the prolonged residence of the ooid within the sediment pile, as light access is limited or unavailable. If ooids are transported to the interdune zones stabilized by seagrass, the sleeping stage may last for an extensive period of time. It seems likely that, in this case, only dune migration may lead to a reactivation of ooid development.

Reactivation stage – Levels 1–2, corresponding to the euphotic zone

Hydrodynamically-induced dune migration or stir-up by storms results in the (re-)exposure of the ooids to the seafloor and, potentially, into the water column. Due to renewed light availability, microbial communities shift from mainly fungi and organotrophs to cyanobacteria and photosynthetic protists. This stage is characterized by the transition from a horizontal to a vertical orientation of borings, clearly representing the shift in the microendolithic community. The dominant microborers are cyanobacteria, with rare chlorophytes.

Based on the increasing amount of euendolithic assemblages associated with increased bioerosion with depth (cf. Glaub *et al.*, 2001, 2007), it is hypothesized that the production of cortical layers by ACC nucleation outweighs bioerosion only during the suspension/agitation phase in the shallow I–II zones. These two stages are therefore referred to as active ooid growth phases. When the ooids enter the sleeping stage, cortical layer destruction by bioerosion predominates over layer formation. Due to

(shallow) burial and the resulting lower light availability, it is suggested that fungi dominate during the sleeping stage, while microalgae dominate during the agitation, resting and reactivation stages.

On that note, there are fungal metabolisms that can induce increases in alkalinity (for example, physicochemical degassing of respired CO₂; Bindschedler *et al.*, 2016), organic acid oxidation (Guggiari *et al.*, 2011), urea mineralization (Burbank *et al.*, 2011) and nitrate assimilation (Hou *et al.*, 2011), and therefore can potentially contribute to carbonate precipitation. However, according to other studies (e.g. Priess *et al.*, 2000), fungi are also aggressive decomposers of carbonate substrates, to the point where fungi even parasitise algae (Schneider, 1976; Le Campion-Alsumard *et al.*, 1995), a process that is likely to occur during the resting and, especially, during the sleeping stage, as documented by characteristic bioerosion traces. Still, bioerosion cannot be attributed to fungal communities alone, because endolithic cyanobacteria and diatoms actively destroy the cortex by boring into the substrate, and organisms such as aerobic heterotrophic bacteria, aerobic sulphide oxidizers and nitrifying bacteria participate in the erosion of the grain through the production of acids as byproducts of their metabolisms (Diaz *et al.*, 2013a, 2013b, 2014, 2015, 2017).

Another aspect of ooid cortex growth is the occlusion of bore tunnels at a cortex depth of approximately 100 µm, which passively contributes to the ooid cortex. This process, however, does not lead to an increase in cortical mass, as it merely fills the previously drilled holes and, therefore, cannot be described as cortex growth.

Calcified remnants of meniscus-like structures were observed, which consisted entirely of rods (see Fig. 3E and F). These meniscus structures may indicate a former capillary water bridge between two layers of the ooid cortex, suggesting air in a cavity (Flügel, 1979; Folk & Lynch, 2001). However, other studies suggest that organic biofilms in a completely phreatic (saturated) environment can also form a meniscus-like structure, so this observation should not be used as the sole indicator for vadose environments or subaerial exposure (Webb *et al.*, 1999; Hillgärtner *et al.*, 2001). Because of this, menisci in ooid cortices may suggest either inorganic mineralization by precipitation from a pore-water in a supratidal environment or mineralization from biofilm residues serving as nucleation templates, the latter possibility being the more likely (cf. Fig. 4A to B and D to E).

Implications for ooid formation and evolution

The extent to which microorganisms with different light preferences contribute to cortex formation or destruction is still controversial. Previous models (e.g. Davies *et al.*, 1978; Duguid *et al.*, 2010; Diaz *et al.*, 2014, 2017) largely focused on geochemical, geomicrobiological or organomineralogical processes involved in cortex formation without characterizing microendolithic communities on ooid surfaces in terms of their preferred habitats (but see Vogel *et al.*, 2000; Gektidis *et al.*, 2007; Glaub *et al.*, 2007). On that note, few, if any, contributions to the broad field of ooid research address the subject of light penetration into the sediment column and how light availability affects the composition of ooid microbial communities. It is hypothesized that there is permanent competition between contemporary microendolithic borers, EPS biofilm production (for example, by biofilm bacteria, diatoms or cyanobacteria), and the precipitation of ACC (inducing the precipitation of aragonite) from biofilms (Diaz *et al.*, 2017). Microbes (diatoms, cyanobacteria, biofilm bacteria, fungi) produce EPS, which then serve as a nucleation template for rods. This formation mechanism is referred to as biologically influenced organomineralization (cf. Dupraz *et al.*, 2009; Diaz *et al.*, 2017). Besides the EPS-mediated mineralization, microbes could also actively contribute to cortex accretion via metabolic pathways (i.e. photosynthesis, denitrification, sulphate reduction, ammonification and anaerobic sulphate oxidation) that generate alkalinity conditions favourable to carbonate precipitation (Dupraz *et al.*, 2009; Diaz *et al.*, 2014, 2015). Accordingly, ooid cortex formation is facilitated by a mixture of biologically influenced and biologically induced organomineralization processes.

In contrast to this constructive function of microbes during ooid cortex formation, others (e.g. Sumner & Grotzinger, 1993; Duguid *et al.*, 2010) acknowledge the involvement of microbes in ooid evolution but argue for an exclusively destructive role. It follows that these authors distinguish between a phase of cortex formation (abiogenic) and a phase of cortex destruction by microendolithic borers. According to Duguid *et al.* (2010), abiogenic ACC precipitation occurs during a 'stationary phase' (i.e. the stage of cortex formation), whereas microbes such as *Solenita* or *Hyella* contribute solely to cortex layer destruction. Based on their observations,

microbes do not play a primary role in ooid genesis. This does not align with the findings presented here, which suggest that microbes play a role in ooid cortex formation through microbial metabolic pathways (i.e. photosynthesis) and EPS-mediated mechanism – the latter providing nucleation sites for mineral precipitation.

In addition, this study suggests that bioerosion outweighs precipitation only during the sleeping stage ('stationary stage' of Duguid *et al.*, 2010). In this context, it is argued that the term 'sleeping stage' implies a stasis in ooid development. In light of the data presented here, this stage is characterized by active cortex destruction. This raises the question of whether the term sleeping stage is appropriate or should be replaced by the more-appropriate term 'destruction stage'.

On a different note, this study could also hold implications for forming fossil ooids or ooids in environments other than the shallow marine realm (for example, lacustrine and deep marine). If sufficiently preserved, a detailed examination of the microbial communities in the cortex could help to reconstruct the palaeoenvironmental conditions under which fossil ooids formed.

CONCLUSIONS

Features of microbial bioerosion in Holocene ooids from two sampling sites – the Schooner Cays ooid shoals (Great Bahama Bank, Eleuthera, Bahamas) and the Shalil al Ud ooid shoals (Abu Dhabi, United Arab Emirates) – were investigated, and vacuum casting was successfully applied, allowing the precise identification of ichnotaxa and their inferred producer as well as their assignment to different ooid formation stages.

The abundance of microendolithic traces varies greatly between grains, suggesting a fluctuating residence time of the ooids at different surficial or shallow burial stages at both sampling sites. Using ichnotaxa as proxies for residence time on the dune surface or within the sediment column depends on the dominance of bioerosion traces efficiently assigned to heterotrophic fungi or photoautotrophic algae. Work shown here differentiates between a high light zone (Level 1) in the water column and above the sediment surface, a twilight zone (Level 2) at the sediment–water interface, constantly affected by shallow burial and resuspension, and a no light zone (Level 3) inside the dune sediment column, characterized by a prolonged burial with an unspecified lower depth limit that

might extend to several metres. This approach provides insight into the distribution and abundance of euendolithic activity on ooids during the established growth stages.

This paper links: (i) the stages of ooid formation; (ii) light availability at the seafloor and in the uppermost sediment column during each stage; and (iii) the resulting composition and distribution of the succeeding ichnotaxa reflecting different microbial communities on and in the ooids. This allows reconstructing the various formation and destruction cycles of a given ooid. Data shown here differentiate an agitation/suspension stage, a resting stage, a sleeping stage (or 'destruction' stage, as proposed here) and a reactivation stage. When applied systematically and for a statistically significant number of ooids, this approach has significant potential to better understand ooid dune dynamics and temporal changes thereof.

ACKNOWLEDGEMENTS

The authors thank Dr G.E. Webb, Dr B. Kołodziej and an unknown reviewer for constructive criticism and helpful suggestions to improve this study. Sedimentology editors Dr M.G. Mángano and Associate Editor Dr J. Webster are greatly thanked for their guidance and comments. Fieldwork on the Great Bahama Bank and in the Abu Dhabi lagoon was financially supported by DFG Grants FOR 1644 and IM 44/23-1. Open Access funding enabled and organized by Projekt DEAL.

CONFLICT OF INTEREST

The authors declare that they are not aware of any competing financial interests or personal relationships that could have appeared to influence the work reported in this paper.

DATA AVAILABILITY STATEMENT

The data presented in this study are available on request from the corresponding author.

REFERENCES

- Al-Thukair, A.A. and Golubic, S. (1991) New endolithic cyanobacteria from the Arabian Gulf. I. *Hyella immanis* sp. nov. *J. Phycol.*, **27**, 766–780.

- Al-Thukair, A.A., Golubic, S. and Rosen, G. (1994) New endolithic cyanobacteria from the Bahama Bank and the Arabian Gulf. *Hyella Racemus* sp. nov. *J. Phycol.*, **30**, 764–769.
- Amao, A.J. and Al-Ramadan, K. (2018) Discussions on Arabian Gulf ooids. *Carbon. Evap.*, **33**, 683–695.
- Anderson, N.T., Cowan, C.A. and Bergmann, K.D. (2020) A case for the growth of ancient ooids within the sediment pile. *J. Sediment. Res.*, **90**, 843–854.
- Arboit, F., Steuber, T., Mohamad, K., Alsuwaidi, M. and Ceriani, A. (2022) Lost in the wind: an integrated approach for the recognition of mixed clastic–carbonate continental aeolianites. *Sedimentology*, **69**, 2203–2227.
- Ball, M.M. (1967) Carbonate sand bodies of Florida and The Bahamas. *J. Sediment. Res.*, **37**, 556–591.
- Bathurst, R.G.C. (1966) Boring algae, micrite envelopes and lithification of molluscan biosparites. *Geol J.*, **5**, 15–32.
- Bergman, K.L., Westphal, H., Janson, X., Poiriez, A. and Eberli, G.P. (2010) Chapter 2 – controlling parameters on facies geometries of The Bahamas, an isolated carbonate platform environment. In: *Carbonate Depositional Systems: Assessing Dimensions and Controlling Parameters* (Eds Westphal, H., Riegl, B. and Eberli, G.), pp. 5–80. Springer, Dordrecht.
- Bindschedler, S., Cailleau, G. and Verrecchia, E. (2016) Role of fungi in the biomineralisation of calcite. *Minerals*, **6**, 41.
- Budd, L.D.A. and Land, L.S. (1990) Geochemical imprint of meteoric diagenesis in Holocene ooid sands, Schooner Cays, Bahamas; correlation of calcite cement geochemistry with extant groundwaters. *J. Sediment. Res.*, **60**, 361–378.
- Bundsuh, M. and Balog, S.J. (2000) *Fasciculus rogos* nov. isp., an endolithic trace fossil. *Ichnos*, **7**, 149–152.
- Burbank, M.B., Weaver, T.J., Green, T.L., Williams, B.C. and Crawford, R.L. (2011) Precipitation of calcite by indigenous microorganisms to strengthen liquefiable soils. *Geomicrobiol. J.*, **28**, 301–312.
- Cartaxana, P., Mendes, C.R., Van Leeuwe, M.A. and Brotas, V. (2006) Comparative study on microphytobenthic pigments of muddy and sandy intertidal sediments of the Tagus estuary. *Estuar. Coast. Shelf Sci.*, **66**, 225–230.
- Colijn, F. and De Jonge, V.N. (1984) Primary production of microphytobenthos in the Ems-Dollard Estuary. *Mar. Ecol. Prog. Ser.*, **14**, 185–196.
- Davies, P.J., Bubela, B. and Ferguson, J. (1978) The formation of ooids. *Sedimentology*, **25**, 703–731.
- del Giorgio, P.A. and Peters, R.H. (1994) Patterns in planktonic P: R ratios in lakes: influence of lake trophic and dissolved organic carbon. *Limnol. Oceanogr.*, **39**, 772–787.
- Diaz, M.R. and Eberli, G.P. (2019) Decoding the mechanism of formation in marine ooids: a review. *Earth Sci. Rev.*, **190**, 536–556.
- Diaz, M.R., Eberli, G.P., Blackwelder, P., Philipps, B. and Swart, P.K. (2017) Microbially mediated organomineralization in the formation of ooids. *Geology*, **45**, 771–774.
- Diaz, M.R., Piggot, A.M., Eberli, G.P. and Klaus, J.S. (2013a) Bacterial community of oolitic carbonate sediments of The Bahamas Archipelago. *Mar. Ecol. Prog. Ser.*, **485**, 9–24.
- Diaz, M.R., Swart, P.K., Devlin, Q., Oehlert, A.M., Saied, A., Eberli, G.P., Klaus, J. and Altabet, M. (2013b) Microbial signature in ooids from The Bahamas. *AGU Fall Meeting*, p. B13E-0554.
- Diaz, M.R., Swart, P.K., Eberli, G.P., Oehlert, A.M., Devlin, Q., Saied, A. and Altabet, M.A. (2015) Geochemical evidence of microbial activity within ooids. *Sedimentology*, **62**, 2090–2112.
- Diaz, M.R., Van Norstrand, J.D., Eberli, G.P., Piggot, A.M., Zhou, J. and Klaus, J.S. (2014) Functional gene diversity of oolitic sands from Great Bahama Bank. *Geobiology*, **12**, 231–249.
- Dravis, J. (1979) Rapid and widespread generation of recent oolitic hardgrounds on a high energy Bahamian platform, Eleuthera Bank, Bahamas. *J. Sediment. Res.*, **49**, 195–207.
- Duguid, S.M.A., Kyser, T.K., James, N.P. and Rankey, E.C. (2010) Microbes and Ooids. *J. Sediment. Res.*, **80**, 236–251.
- Dupraz, C., Reid, R.P., Braissant, O., Decho, A.W., Norman, R.S. and Visscher, P.T. (2009) Processes of carbonate precipitation in modern microbial mats. *Earth Sci. Rev.*, **96**, 141–162.
- Edinger, E.N., Copper, S.P., Risk, M.J. and Atmojo, W. (2002) Oceanography and reefs of recent and Paleozoic tropical epeiric seas. *Facies*, **47**, 127–149.
- Evans, G., Schmidt, V., Bush, P. and Nelson, H. (1969) Stratigraphy and geological history of the Sabkha, Abu Dhabi, Persian Gulf. *Sedimentology*, **12**, 145–159.
- Fenchel, T. and Straarup, B.J. (1971) Vertical distribution of photosynthetic pigments and the penetration of light in marine sediments. *Oikos*, **22**, 172–182.
- Flügel, E. (1979) Paleoeology and microfacies of Permian, Triassic and Jurassic algal communities of platform and reef carbonates from the alps. *Bull. Cent. Rech. Explor.*, **2**, 569–587.
- Flügel, E. and Munnecke, A. (2010) *Microfacies of Carbonate Rocks – Analysis, Interpretation and Application*. Springer, Berlin Heidelberg; New York, 454 pp.
- Folk, R.L. and Lynch, F.L. (2001) Organic matter, putative nannobacteria and the formation of ooids and hardgrounds. *Sedimentology*, **48**, 215–229.
- Försterra, G., Beuck, L., Häussermann, V. and Freiwald, A. (2005) Shallow-water *Desmophyllum dianthus* (Scleractinia) from Chile: characteristics of the biocoenoses, the bioeroding community, heterotrophic interactions and (paleo)-bathymetric implications. In: *Cold-water Corals and Ecosystems* (Eds Freiwald, A. and Roberts, J.M.), pp. 937–977. Springer-Verlag, Berlin, Heidelberg.
- Friedman, G.M., Gebelein, C.D. and Sanders, J.E. (1971) Micritic envelopes of carbonate grains are not exclusively of photosynthetic algal origin. *Sedimentology*, **16**, 89–96.
- Gaffey, S. (1983) Formation and infilling of pits in marine ooid surfaces. *J. Sediment. Res.*, **53**, 193–208.
- García-Pichel, F., Ramírez-Reinat, E. and Gao, Q. (2010) Microbial excavation of solid carbonates powered by P-type ATPase-mediated transcellular Ca²⁺ transport. *Proceedings of the National Academy of Sciences of the United States of America*, **107**, 21749–21754.
- Ge, Y., Lokier, S.W., Hoffmann, R., Pederson, C.L., Neuser, R.D. and Immenhauser, A. (2020b) Composite micrite envelopes in the lagoon of Abu Dhabi and their application for the recognition of ancient firm- to hardgrounds. *Marine Geology*, **423**, 106141.
- Ge, Y., Pederson, C.L., Lokier, S.W., Traas, J.P., Nehrke, G., Neuser, R.D., Goetschl, K.E. and Immenhauser, A. (2020a) Late Holocene to Recent aragonite-cemented transgressive lag deposits in the Abu Dhabi lagoon and intertidal sabkha. *Sedimentology*, **67**, 2426–2454.
- Gektidis, M. (1997) Microbioerosion in Bahamian ooids. *Cour. Forsch. Inst. Senckenberg*, **201**, 109–121.
- Gektidis, M., Dubinsky, Z. and Goffredo, S. (2007) Microendoliths of the Shallow Euphotic Zone in open and shaded habitats at 30° N – Eilat, Israel – paleoecological implications. *Facies*, **53**, 43–55.

- Glaub, I.** (1994) Mikrobohrspuren in ausgewählten Ablagerungsräumen des europäischen Jura und der Unterkreide (Klassifikation und Palökologie). *Cour. Forsch. Inst. Senckenberg*, **174**, 1–324 (in German with English abstract).
- Glaub, I.** (2004) Recent and sub-recent microborings from the upwelling area off Mauritania (West Africa) and their implications for palaeoecology. *Geol. Soc. Spec. Publ.*, **228**, 63–76.
- Glaub, I. and Bundschuh, M.** (1997) Comparative studies on Silurian and Jurassic/Lower Cretaceous microborings. *Cour. Forsch. Inst. Senckenberg*, **201**, 123–135.
- Glaub, I., Golubic, S., Gektidis, M., Radtke, G. and Vogel, K.** (2007) Chapter 21 – microborings and microbial endoliths: geological implications. In: *Trace Fossils - Concepts, Problems, Prospects* (Ed. Miller III, W.), pp. 368–381. Elsevier Science, Oxford.
- Glaub, I., Vogel, K. and Gektidis, M.** (2001) The role of modern and fossil cyanobacterial borings in bioerosion and bathymetry. *Ichnos*, **8**, 185–195.
- Goldstein, J.I., Newbury, D.E., Michael, J.R., Ritchie, N.W.M., Scott, J.H.J. and Joy, D.C.** (2017) *Scanning Electron Microscopy and X-Ray Microanalysis*, pp. 481–490. Springer, New York.
- Golubic, S., Campbell, S.E., Drobne, K., Cameros, B., Balsam, W.L., Cimerman, F. and Dubios, L.** (1984) Microbial Endoliths: a benthic overprint in the sedimentary record, and a Paleobathymetric cross-reference with foraminifera. *J. Paleo.*, **58**, 251–361.
- Golubic, S., Campbell, S.E., Lee, S.J. and Radtke, G.** (2016) Depth distribution and convergent evolution of microboring organisms. *PalZ*, **90**, 315–326.
- Golubic, S., Friedmann, I. and Schneider, J.** (1981) The Lithobiontic ecological niche, with special reference to microorganisms. *J. Sediment. Petrol.*, **51**, 475–478.
- Golubic, S., Perkins, R.D. and Lukas, K.J.** (1975) Boring microorganisms and microborings in carbonate substrates. In: *The Study of Trace Fossils* (Ed Frey, R.W.), pp. 229–259. Springer, Berlin, Heidelberg.
- Gomiou, M.T.** (1967) Some quantitative data on light penetration in sediment. *Helgol Wiss Meeresunters*, **15**, 120–127.
- Guggiari, M., Bloque, R., Aragno, M., Verrecchia, E., Job, D. and Junier, P.** (2011) Experimental calcium-oxalate crystal production and dissolution by selected wood-rot fungi. *Int. Biodeter. Biodegr.*, **65**, 803–809.
- Harris, P.M.** (1983) The Joulters Ooid Shoal, Great Bahama Bank. In: *Coated Grains* (Ed Peryt, T.M.), pp. 132–141. Springer, Berlin, Heidelberg.
- Harris, P.M.** (2010) Delineating and quantifying depositional facies patterns in carbonate reservoirs: Insight from modern analogs. *Am. Assoc. Pet. Geol. Bull.*, **94**, 61–86.
- Harris, P.M., Diaz, M.R. and Eberli, G.P.** (2019) The formation and distribution of modern Ooids on Great Bahama Bank. *Ann. Rev. Mar. Sci.*, **11**, 491–516.
- Harris, P.M., Halley, R.B. and Lukas, K.** (1979) Endolith microborings and their preservation in Holocene-Pleistocene (Bahama-Florida) ooids. *Geology*, **7**, 216–220.
- Harris, P.M., Purkis, S.J. and Ellis, J.** (2011) Analysing spatial patterns in modern carbonate sand bodies from Great Bahama Bank. *J. Sediment. Res.*, **81**, 185–206.
- Harris, P.M., Purkis, S.J. and Ellis, J.** (2014) Evaluating water-depth variation and mapping depositional facies on Great Bahama Bank – a “flat-topped” isolated carbonate platform. *SEPM Short Course*, **56**, 1–44.
- Hillgärtner, H., Dupraz, C. and Hug, W.** (2001) Microbially induced cementation of carbonate sands: are micritic meniscus cements good indicators of vadose diagenesis? *Sedimentology*, **48**, 117–131.
- Hoffmann, R., Richter, D.K., Neuser, R.D., Jöns, N., Linzmeier, B.J., Lemanis, R.E., Fusses, F., Xiao, X. and Immenhauser, A.** (2016) Evidence for a composite organic–inorganic fabric of belemnite rostra: implications for palaeoceanography and palaeoecology. *Sed. Geol.*, **341**, 203–215.
- Hou, W., Lian, B. and Zhang, X.** (2011) CO₂ mineralisation induced by fungal nitrate assimilation. *Bioresour. Technol.*, **102**, 1562–1566.
- Ichimi, K., Tada, K. and Montani, S.** (2008) Simple estimation of penetration rate of light in intertidal sediments. *J. Oceanogr.*, **64**, 399–404.
- Kalkowsky, E.** (1908) Oolith und Stromatolith im norddeutschen Buntsandstein. *Z. Dtsch. Geol. Ges.*, **60**, 68–125.
- Kinsman, D.J.J.** (1964) The Recent Carbonate Sediments near Halat El Bahrani, Trucial Coast, Persian Gulf. In: *Deltaic and Shallow Marine Deposits Proceedings of the 6th International Sedimentological Congress The Netherlands and Belgium – 1963* (Ed Van Straaten, L.M.J.U.), pp. 185–192. Elsevier, Amsterdam.
- Kühl, M., Lassen, C. and Jørgensen, B.B.** (1994) Light penetration and light intensity in sandy marine sediments measured with irradiance and scalar irradiance fiber-optic microprobes. *Mar. Ecol. Prog. Ser.*, **105**, 139–148.
- Le Campion-Alsumard, T., Golubic, S. and Priess, K.** (1995) Fungi in Corals: symbiosis or disease? Interaction between polyps and fungi causes pearl-like skeleton biomineralisation. *Mar. Ecol. Prog. Ser.*, **117**, 137–147.
- Li, F., Yan, J., Chen, Z.Q., Ogg, J.G., Tian, L., Korngreen, D., Liu, K., Ma, Z. and Woods, A.D.** (2015) Global oolite deposits across the Permian–Triassic boundary: a synthesis and implications for palaeoceanography immediately after the end-Permian biocrisis. *Earth Sci. Rev.*, **149**, 163–180.
- Lokier, S.W. and Fiorini, F.** (2016) Temporal evolution of a carbonate coastal system, Abu Dhabi, United Arab Emirates. *Mar. Geol.*, **381**, 102–113.
- Macintyre, I.G., Prufert-Bebout, L. and Reid, R.P.** (2000) The role of endolithic cyanobacteria in the formation of lithified laminae in Bahamian stromatolites. *Sedimentology*, **47**, 915–921.
- Margolis, S. and Rex, R.W.** (1971) Endolithic algae and micrite envelope formation in Bahamian oolites as revealed by scanning electron microscopy. *Geol. Soc. Am. Bull.*, **82**, 843–852.
- Mariotti, G., Pruss, S.B., Summons, R.E., Newman, S.A. and Bosak, T.** (2018) Contribution of benthic processes to the growth of ooids on a low-energy shore in Cat Island, The Bahamas. *Minerals*, **8**, 252.
- May, J.A. and Perkins, R.D.** (1979) Endolithic algae and micrite envelope formation in bahamian oolites as revealed by scanning electron microscopy. *Geol. Soc. Am. Bull.*, **82**, 843–852.
- McCutcheon, J., Nothdurft, L.D., Webb, G.E., Paterson, D. and Southam G.** (2016) Beachrock formation via microbial dissolution and re-precipitation of carbonate minerals. *Mar. Geol.*, **382**, 122–135.
- Milliman, J.D., Müller, G. and Förstner, U.** (1974) *Recent Sedimentary Carbonates: Part 1 Marine Carbonates*. Springer Science & Business Media, Berlin, Heidelberg, 378 pp.
- Opdyke, B.N. and Wilkinson, B.H.** (1990) Palaeolatitude distribution of Phanerozoic marine ooids and cements. *Palaeoceanogr. Palaeoclimatol. Palaeoecol.*, **78**, 135–148.

- Pederson, C.L., Ge, Y., Lokier, S.W., Swart, P.K., Vohnhof, H., Strauss, H., Schurr, S., Fiorini, F., Riechelmann, S., Licha, T. and Immenhauser, A.** (2021) Seawater chemistry of a modern subtropical 'epeiric' sea: spatial variability and effects of organic decomposition. *Geochim. Cosmochim. Acta*, **314**, 159–177.
- Pinckney, J. and Zingmark, R.G.** (1993) Photophysiological responses of intertidal benthic microalgal communities to *in situ* light environments: methodological considerations. *Limnol. Oceanogr.*, **38**, 1373–1383.
- Popp, B.N. and Wilkinson, B.H.** (1983) Holocene lacustrine ooids from Pyramid lake, Nevada. In: *Coated Grains* (Ed Peryt, T.M.), pp. 142–153. Springer, Berlin, Heidelberg.
- Priess, K., Le Champion-Alsumard, T., Golubic, S., Gadel, F. and Thomassin, B.A.** (2000) Fungi in corals: black bands and density-banding of *Porites lutea* and *P. lobata* skeleton. *Mar. Biol.*, **136**, 19–27.
- Purkis, S.J. and Harris, P.M.** (2017) Quantitative interrogation of a fossilised carbonate sand body – the Pleistocene Miami oolite of South Florida. *Sedimentology*, **64**, 1439–1464.
- Purkis, S.J., Harris, P.M. and Cavalcante, G.** (2019) Controls of depositional facies patterns on a modern carbonate platform: insight from hydrodynamic modelling. *Depos. Rec.*, **5**, 421–437.
- Radtke, G.** (1991) Die mikroendolithischen Spurenfossilien im Alt-Tertiär-West-Europas und ihre palökologische Bedeutung. *Cour. Forsch. Inst. Senckenberg*, **138**, 1–150.
- Radtke, G. and Golubic, S.** (2011) Microbial euendolithic assemblages and microborings in intertidal and shallow marine habitats: insight in cyanobacterial speciation. In: *Advances in Stromatolite Geobiology* (Eds Reitner, J., Quéric, N.V. and Arp, G.), *LNES*, **131**, 233–263.
- Rankey, E.C. and Reeder, S.L.** (2011) Holocene oolitic marine sand complexes of The Bahamas. *J. Sediment. Res.*, **81**, 97–117.
- Rankey, E.C. and Reeder, S.L.** (2012) Tidal sands of the Bahamian archipelago. In: *Principles of Tidal Sedimentology* (Eds Davis, R., Jr. and Dalrymple, R.), pp. 537–565. Springer, Dordrecht.
- Rankey, E.C., Riegel, B. and Steffen, K.** (2006) Form, function and feedbacks in a tidally dominated ooid shoal, Bahamas. *Sedimentology*, **53**, 1191–1210.
- Reeder, S.L. and Rankey, E.C.** (2008) Interactions between tidal flows and Ooid Shoals, Northern Bahamas. *J. Sediment. Res.*, **78**, 175–186.
- Reid, R.P. and Macintyre, I.G.** (2000) Microboring versus recrystallisation: further insight into the micritisation process. *J. Sediment. Res.*, **70**, 24–28.
- Richter, D.K.** (1983) Calcareous ooids: a synopsis. In: *Coated Grains* (Ed Peryt, T.M.), pp. 71–99. Springer-Verlag, New York.
- Richter, D.K. and Neuser, R.D.** (1998) Marine aragonite-ooids and brackish Mg-calcite-ooids in "Neogene"-Pleistocene cycles of the section of the Canal of Corinth, Greece. *Bulletin Geol. Soc. Greece*, **32**, 277–287.
- Rush, J.W. and Rankey, E.C.** (2017) Geostatistical facies modeling trends for oolitic tidal sand shoals. *Am. Assoc. Pet. Geol. Bull.*, **101**, 1341–1379.
- Salamon, K. and Kołodziej, B.** (2022) Unravelling the microbiome of fossil corals: a message from microborings. *Hist. Biol.*, **34**, 1228–1239.
- Salamon, K., Kołodziej, B. and Stefanskyi, V.L.** (2019) Simple methods for detection of microborings produced by coral-associated microendoliths. *Facies*, **65**, 16.
- Sandberg, P.** (1983) An oscillating trend in Phanerozoic non-skeletal carbonate mineralogy. *Nature*, **305**, 19–22.
- Sandberg, P.A.** (1975) New interpretations of Great Salt Lake ooids and of ancient non-skeletal carbonate mineralogy. *Sedimentology*, **22**, 497–537.
- Schätzle, P.-K., Wisshak, M., Bick, A., Freiwald, A. and Kieneke, A.** (2021) Exploring confocal laser scanning microscopy (CLSM) and fluorescence staining as a tool for imaging and quantifying traces of marine microbioerosion and their trace-making microendoliths. *J. Microsc.*, **284**, 118–131.
- Schmidt, H.** (1992) Mikrobohrspuren ausgewählter Faziesbereiche der tethyalen und germanischen Trias (Beschreibung, Vergleich und bathymetrische Interpretation). *Frankfurter Geowissenschaftliche Arbeiten*, **12**, 1–228.
- Schneider, J.** (1976) Biological and inorganic factors in the destruction of limestone coasts. *Contrib Sedimentol.*, **6**, 1–112.
- Scholle, P.A. and Ulmer-Scholle, D.S.** (2003) Chapter 14 – GRAINS: Non-skeletal Grains Ooids, Pisoids and other coated grains. In: *A Color Guide to the Petrography of Carbonate Rocks: Grains, Textures, Porosity, Diagenesis* (Eds Scholle, P.A. and Ulmer-Scholle, D.S.), pp. 227–244. The American Association of Petroleum Geologists, Tulsa, OK.
- Simone, L.** (1980) Ooids: a review. *Earth Sci. Rev.*, **16**, 319–355.
- Sorby, H.C.** (1879) The structure and origin of limestones. *Pop. Sci. Rev.*, **3**, 134–137.
- Stevens, T., Jestico, M.J., Evans, G. and Kirkham, A.** (2014) Eustatic control of late Quaternary sea-level change in the Arabian/Persian Gulf. *Quatern. Res.*, **82**, 175–184.
- Suarez-Gonzalez, P. and Reitner, J.** (2021) Ooids forming in situ within microbial mats (Kiritimati atoll, central Pacific). *PalZ*, **95**, 809–821.
- Sullivan, M.J. and Moncreiff, C.A.** (1988) Primary production of edaphic algal communities in a Mississippi salt marsh. *J. Phycol.*, **24**, 49–58.
- Sumner, D.Y. and Grotzinger, J.P.** (1993) Numerical modelling of ooid size and the problem of Neoproterozoic giant ooids. *J. Sediment. Res.*, **63**, 974–982.
- Tapanila, L.** (2008) The endolithic guild: an ecological framework for residential cavities in hard substrates. In: *Current Developments in Bioerosion* (Eds Wisshak, M. and Tapanila, L.), pp. 3–20. Springer, Berlin, Heidelberg.
- Vogel, K., Bundschuh, M., Glaub, I., Hofmann, K., Radtke, G. and Schmidt, H.** (1995) Hard substrate ichnocoenoses and their relations to light intensity and marine bathymetry. *Neues Jahrb. Geol. Palaontol. Abh.*, **195**, 49–61.
- Vogel, K., Gektidis, M., Golubic, S., Kiene, W.E. and Radtke, G.** (2000) Experimental studies on microbial bioerosion at Lee Stocking Island, Bahamas and One Tree Island, Great Barrier Reef, Australia: Implications for paleoecological reconstructions. *Lethaia*, **33**, 190–204.
- Vogel, K., Golubic, S. and Brett, C.E.** (1987) Endolith associations and their relation to facies distribution in the Middle Devonian of New York State, USA. *Lethaia*, **20**, 263–290.
- Vogel, K., Kiene, W.E., Gektidis, M. and Radtke, G.** (1996) Scientific results from investigation of microbial borers and bioerosion in reef environments. In: *Global and Regional Controls on Biogenic Sedimentation. I. Reef Evolution* (Eds Reitner, J., Neuweiler, F. and Gunkel, F.), *Research reports, Göttinger Arb Geol Pal*, **2**, 139–143.
- Webb, G.E., Jell, J.S. and Baker, J.C.** (1999) Cryptic intertidal microbialites in beachrock, Heron Island, Great Barrier Reef: implications for the origin of microcrystalline beachrock cement. *Sed. Geol.*, **126**, 317–334.

- Whitaker, F.F. and Smart, P.L. (1990) Active circulation of saline ground waters in carbonate platforms: evidence from the Great Bahama Bank. *Geology*, **18**, 200–203.
- Wisshak, M. (2012) Chapter 8 – Microbioerosion. *Dev. Sediment.*, **64**, 213–243.
- Wisshak, M., Knaust, D. and Bertling, M. (2019) Bioerosion Ichnotaxa: review and annotated list. *Facies*, **65**, 24.
- Wisshak, M., Tribollet, A., Golubic, S., Jakobsen, J. and Freiwald, A. (2011) Temperate bioerosion: ichnodiversity and biodiversity from intertidal to bathyal depths (Azores). *Geobiology*, **9**, 492–520.
- Yallop, M.L., de Winder, B., Paterson, D.M. and Stal, L.J. (1994) Comparative structure, primary production and biogenic stabilisation of cohesive and non-cohesive marine sediments inhabited by microphytobenthos. *Estuar. Coast. Shelf Sci.*, **39**, 565–582.

Manuscript received 13 March 2023; revision accepted 13 October 2023

Supporting Information

Additional information may be found in the online version of this article:

Appendix S1. Methods.

Appendix S2. Raman measurements Bahamas, Schooner Cays ooids.

Appendix S3. Raman measurements Abu Dhabi, Shalil al Ud ooids.

Fig. S1. Transmitted light (TL) (A) and (D), cross-polars (pol. X) (B) and (E) and cathodoluminescence (CL) (C) and (F) of the ooid sand from Shalil al Ud (the Gulf; size class 1 to 0.63 mm). Composite ooids can comprise two (A; light green arrow) or more (D;

dark green arrow) ooids, connected by micritic cements and often enveloped in new layers. Superficial grains with various nuclei (A, D; lilac arrows) occur more frequently than typical ooids with thick cortices. The latter portray a pseudo-uniaxial extinction cross (B; light green arrow). In some void volumes acicular crystals have developed (A, D; yellow arrows). Cements appear in a patchy brown colour, while intact shell fragments appear white when observed under pol. X, similar to TL observations. Under CL, several components as well as the cement forming at grain margins, portray light to dark orange colours (E, F; light blue arrows). The cortices of ooids (for example, A; green arrow) luminesce in a dark blue colour, among the majority of micritic cements, gastropod shells and some of the unidentified bioclasts. A small amount of fragments or crystals luminesce in dull green colours (C, F; orange arrows).

Fig. S2. Transmitted light (TL) (A) and (D), cross-polars (pol. X) (B) and (E) and cathodoluminescence (CL) (C) and (F) of the ooid sand from the Schooner Cays (size class 1 to 0.63 mm). Superficial ooids with rather thin cortices (A, D; lilac arrows) predominate. Composite ooids enveloped by micritic cements occur infrequently (A, D; light green arrows). A convergence towards a spherical form, is achieved by layers replenishing notches in nuclei (A; lilac arrow). Skeletal grains (foraminifera; A, D; pink arrows) can serve as nuclei besides peloids (for example, D; orange arrow). Micritic cement appears in patchy brown (TL, pol. X), while intact shell fragments appear white or grey (pearlescent under pol. X). Intact ooid layers show birds eyes (B, E; blue arrows). Some (composite) grains consist of two distinct materials with different luminescence behaviour (F; red circle). (Micritic) cements at grain margins are luminescing in dark blue (F; yellow arrow) or bright orange, (C, F; light blue arrows). The cortices show dark blue colours (C, F; blue arrows).